Predicting nonlinear physical aging of glasses from equilibrium relaxation via the material time

Birte Riechers, Lisa A. Roed, Saeed Mehri, Trond S. Ingebrigtsen, Tina Hecksher, Jeppe C. Dyre, Kristine Niss[1]

[1] *"Glass and Time", IMFUFA, Dept. of Science and Environment, Roskilde University, P. O. Box 260, DK-4000 Roskilde, Denmark*

(Dated: September 27, 2021)

The noncrystalline glassy state of matter plays a role in virtually all fields of material science and offers complementary properties to those of the crystalline counterpart. The caveat of the glassy state is that it is out of equilibrium and therefore exhibits physical aging, i.e. the material properties change over time. For half a century the physical aging of glasses has been known to be described well by the material-time concept, though the existence of a material time has never been directly validated. We do this here by successfully predicting the nonlinear aging of the molecular glass 4-vinyl-1,3-dioxolan-2-one from its linear relaxation behavior. This establishes the defining property of the material time. Via the fluctuation-dissipation theorem our results imply that physical aging can be predicted from thermal-equilibrium fluctuation data and we confirm this by computer simulations of a binary model liquid.

Physical aging deals with small property changes resulting from structural rearrangements [1–5]. While the aging of a material is in practice often due to chemical degradation, physical aging does not involve any chemical change. Understanding this type of aging is crucial for applications of noncrystalline materials like oxide glasses [4, 6, 7], polymers [2, 5, 8–10], metallic glasses [11–13], amorphous pharmaceuticals [14], colloidal suspensions [15], etc. For instance, the performance of a smartphone display glass is controlled by details of the physical aging during production [16], and some plastics eventually become brittle as a result of physical aging [17]. Noncrystalline or partly noncrystalline states also play a role in modern material science, e.g. metal organic frameworks [18] and high entropy alloys [19]. The lack of fundamental understanding of the glassy state therefore influences all branches of material science.

Describing and predicting physical aging has been a focus of glass science for many years, yet the subject still presents challenges [10, 20]. We here address the fundamental concept of a material ("reduced") time controlling aging, which was proposed by Narayanaswamy in 1971 in a paper dealing with the physical aging of oxide glasses [6]. A closely related formalism describing polymer aging was developed a few years later by Kovacs and coworkers [3] and, in the 1990s, in the entirely different context of spin glasses by Cugliandolo and Kurchan [21]. The material-time concept rationalizes several striking aging phenomena [4, 6, 22–24]. It is used routinely in both basic research and applications, and the material-time formalism is generally recognized to describe well the physical aging of systems subjected to relatively small temperature variations. The existence of a material time has never been validated in direct experiments, however. We do this here in long-time experiments on a glass-forming molecular liquid by demonstrating the fundamental prediction that linear-response aging data determine the nonlinear aging behavior.

Physical aging is a complex phenomenon because it is both nonexponential and nonlinear. The simplest and best controlled aging experiment is a temperature jump protocol: the sample is initially in a state of thermal, then its temperature is changed instantaneously (i.e., rapidly compared to the response time scale of the material) and the full approach to equilibrium at the new temperature is monitored as a function of time [25]. Doing this requires a setup that allows for fast temperature changes and has a precise temperature control with minimal long-time drift. Moreover, accurate measurements are needed because the long-time-tail of physical aging and the entire aging response to a small temperature step involve only minute changes of material properties. Our experimental setup is based on a Peltier element in direct contact with a thin-sample plane-plate capacitor. The setup keeps temperature constant over months with less than 1 mK variation, and the samples are so thin (50 μm) that temperature may be changed within a few seconds to a new, constant value. Dielectric properties are monitored using an ultra-precision Andeen-Hagerling A2700 capacitance bridge. More details on the setup are provided in Refs. 25–29.

We performed several temperature-jump experiments around a reference temperature on the glass-forming liquid 4-vinyl-1,3-dioxolan-2-one (VEC) and monitored, after each jump, both the real and the imaginary part of the capacitance at 10 kHz as the system gradually equilibrates [30, 31]. The real part of the VEC data is presented in Fig. 1; the imaginary part data can be found in the Supplementary Materials in which we also give analogous data for N-methyl-ε-caprolactam (NMEC). Capacitance can be measured very precisely and is a good probe in aging experiments [25, 32, 33]. For samples of molecules with a low dipole moment, the real part of the capacitance provides a measure of the density [27]. VEC and NMEC molecules have both large dipole moments, however, which implies that rotational polarizations contribute significantly to the capacitance even at high frequencies [27, 34]. This means that the simple connection to density is lost, but the capacitance still provides a precise probe of the state of the sample during aging.

The reference temperature for the VEC experiment is 164.6 K at which the relaxation time is roughly 12 hours (see the Supplementary Materials). This is large enough for the setup to thermalize after a temperature jump before any significant relaxation has taken place. Figure 1A shows our temperature protocol (upper panel) with the 10 kHz real part of the capacitance measured as a function of time (lower panels). The first 36 weeks of the experiment were mainly devoted to single temperature jumps with size varying from 10 mK to 3 K, carefully equilibrating the sample after each jump before the next one was initiated. The last 15 weeks were spent on temperature variations involving double jumps and sinusoidal modulations. The latter are not resolved in this figure where they appear as thick turquoise vertical lines; we return to these protocols later (Figs. 2 and 3). Figure 1B shows the data for the single jumps plotted as a function of the logarithm of the time since each jump was initiated. Note that these curves have very different shapes. This demonstrates that even fairly small temperature jumps lead to a significantly nonlinear response. This is a hallmark of physical aging, reflecting the "asymmetry of approach" that jumping to the same final temperature from a higher temperature results in a faster and more stretched response than the same-size jump coming from below [4, 6, 10, 35]. Figure 1C focuses on the smaller jumps that are not resolved in Fig. 1B.

The physical aging response to a temperature variation is usually highly nonlinear. Nevertheless, any response is expected to

have a small-amplitude limit at which the measured quantity, $X(t)$, depends linearly on the external perturbation. Even in this linear limit the system still has a memory, and thus the measured signal depends on the entire temperature-input history. This implies that $X(t)$ in the linear limit is given by a convolution of the change in temperature with a normalized linear time-domain response function $R_{\mathrm{lin}}(t)$ in the following manner:

$$X(t) - X_{\mathrm{eq}}(T) = -\alpha_X \int_{-\infty}^{t} R_{\mathrm{lin}}(t-t') \frac{dT}{dt'} dt' \,. \tag{1}$$

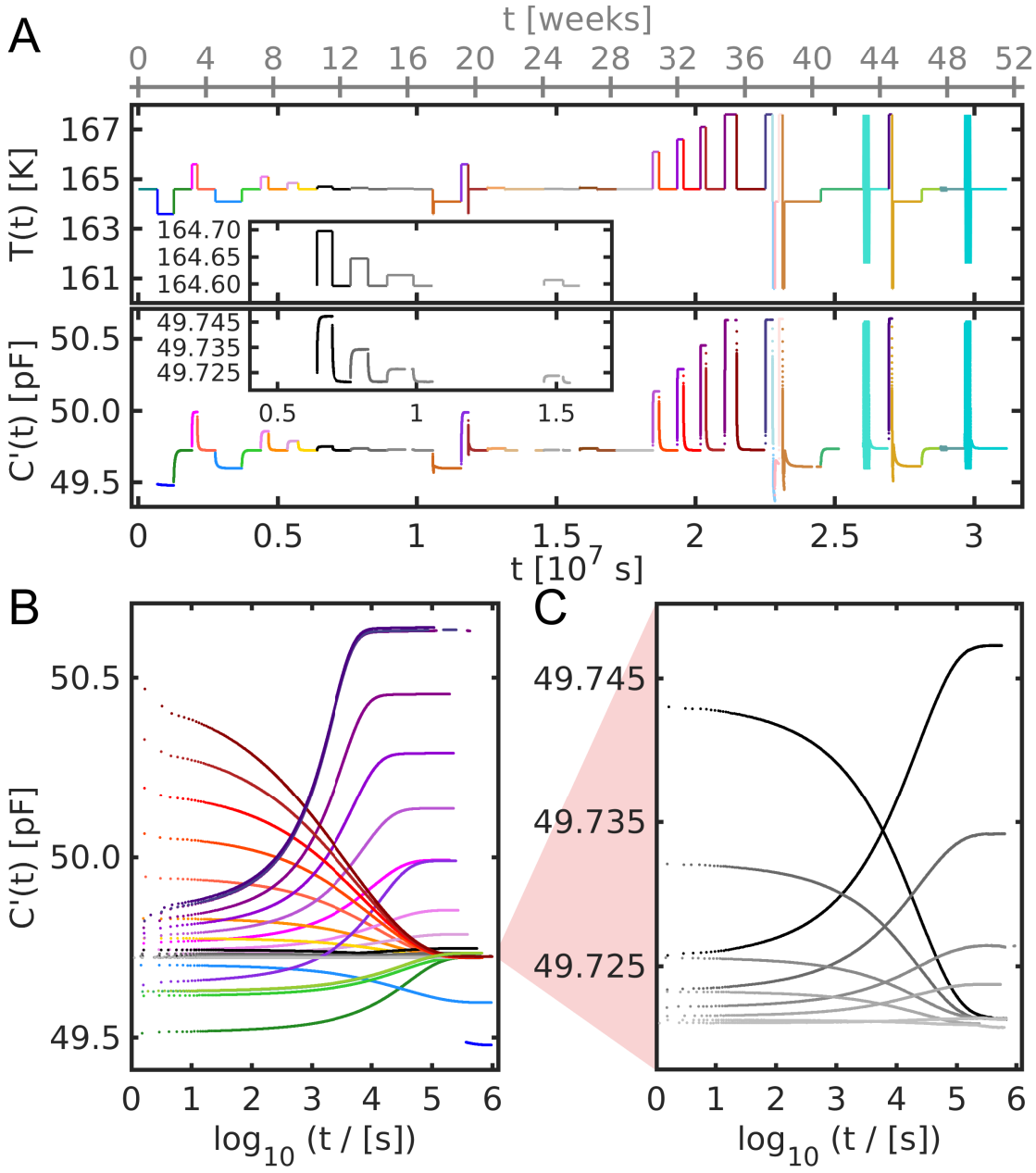

FIG. 1: Overview of the temperature protocol and the raw data of the full experiment on VEC. A The experimental protocol realized by small temperature modulations around the reference temperature 164.6 K (upper panel) and the real part of the measured capacitance $C'(10\,\mathrm{kHz})$ (lower panel), both plotted as functions of time on a linear scale. Jumps larger than 100 mK are colored while jumps of 100 mK or less are depicted on a grey scale; a selection of the latter is shown in the inset. Sinusoidal temperature modulations also studied (see below) are not resolved in this figure where they appear as turquoise thick vertical lines. B The capacitance $C'(10\,\mathrm{kHz})$ data plotted as functions of the logarithm of the time t that has passed after each jump. C Zoom in on the data of the jumps of magnitude 100 mK or less.

Here the temperature T is in general a function of the time t. $X_{\rm eq}(T)$ is the equilibrium value of the measured property at temperature T and $\alpha_X = dX_{\rm eq}/dT$ quantifies its temperature dependence. This type of linear behavior is also known as the Boltzmann superposition principle – a term often used in rheology. In the case of a temperature jump at time zero from the initial temperature T_i to the final temperature T_f one has $dT/dt' = \Delta T\,\delta(t')$ in which $\Delta T = T_f - T_i$, and Eq. 1 implies that the time-dependent response is equal to $-\alpha_X \Delta T R_{\rm lin}(t)$. Defining $\Delta X = X_{\rm eq}(T_i) - X_{\rm eq}(T_f)$ and noting that $\Delta X = -\alpha_X \Delta T$, the response is given by

$$X(t) - X_{\rm eq}(T_f) = \Delta X R_{\rm lin}(t) \tag{2}$$

Previously we have worked with this linear limit with temperature jumps down to 100 mK [27–29, 36]; the data of the present paper takes this a step further by involving temperature jumps as small as 10 mK, as well as by optimizing the protocol to make it possible for the first time properly to resolve both the long- and the short-time plateaus of the linear aging curve.

Linearity is investigated by considering the normalized relaxation function of the quantity X, denoted by $R_X(t)$, which for a temperature jump at $t = 0$ is defined by

$$R_X(t) \;=\; \frac{X(t) - X_{\rm eq}(T_f)}{\Delta X}\,. \tag{3}$$

Clearly $R_X(0) = 1$ and $R_X(t)$ goes to zero as the system equilibrates at T_f at long times. If the data are linear, the relaxation function is given by the response function of Eq. 1, $R_X(t) = R_{\rm lin}(t)$, implying that relaxations following different size temperature jumps have the same time-dependent normalized relaxation function.

Fig. 2 shows $R(t)$ for temperature jumps of magnitude 10-100 mK to and from the reference temperature, where $X = C'(10\ \text{kHz})$ is the real part of the capacitance at 10 kHz of VEC. Similar data are shown for the imaginary part and for NMEC in the Supplementary Materials. The short-time plateau of $R(t)$ is below the theoretical value $R(0) = 1$. This is because there is a fast response that cannot be resolved by our setup, a common finding in studies of physical aging. For instance, one or more beta relaxations may take place at times shorter than the experimental cutoff of about 4s (the time it takes to change temperature and equilibrate the setup at the new temperature).

All normalized relaxation functions $R(t)$ observed for these temperature jumps collapse within the experimental uncertainty, as predicted for a linear response. True linearity is a theoretical limit, which means that higher precision and better resolution would reveal tiny differences between the relaxation curves. However, for these data the uncertainty is of the same magnitude as the symbol size and no differences are resolved, meaning that the measured curves for all practical purposes represent the linear-response function $R_{\rm lin}(t)$. In the following we demonstrate how the linear-response function can be used to predict the response for different temperature protocols resulting in linear (Fig. 2) as well as non-linear (Fig. 3) aging responses.

The simplest extension from a single temperature-jump experiment is to introduce a second jump before the system has equilibrated fully in response to the first one, a so-called double-jump experiment. If the temperature changes are both small enough to be within the linear range, the measured value of $X(t)$ after the second jump is a sum of the responses to the individual jumps. For two temperature jumps corresponding to changes in the measured property X by ΔX_1 and ΔX_2 performed at times t_1 and t_2 ($t_1 < t_2$), respectively, one has

$$X(t) = \Delta X_1 R_{\rm lin}(t - t_1) + \Delta X_2 R_{\rm lin}(t - t_2) + X_{\rm eq}(T_2) \text{ for } t > t_2 \tag{4}$$

where T_2 is final temperature after the second jump.

We test Eq. 4 for the Ritland-Kovacs cross-over protocol [4, 35] consisting of two consecutive temperature jumps with opposite sign performed such that the observable X has its equilibrium value right after the second jump. Figure 2B illustrates this protocol and shows the observations after a -100 mK jump followed by a $+50$ mK jump for VEC. The data reproduce the cross-over effect that $X(t)$ exhibits a peak after the second jump [4, 35]. This bump is a direct manifestation of the memory effect present in any nonexponential linear response [4]. Along with the data, the predictions based on Eq. 4 and the measured $R_{\rm lin}(t)$ from the 50 mK jump in Fig. 1A are also shown. The prediction collapses almost exactly with the double-jump data. These small-amplitude double jump results provide an extra confirmation that we have reached the linear limit of physical aging. Similar data are presented for the liquid NMEC in the Supplementary Materials.

Moving on from the double temperature jump, we note that Eq. 1 predicts the response to any temperature perturbation small enough to be linear. Since we do not have an analytic expression for $R_{\rm lin}(t)$, the integral is performed by generalizing the sum in Eq. 4:

$$X(t) = \sum_{i=1}^{N} \Delta X_i R_{\rm lin}(t - t_i) + X_{\rm eq}(T_N) \text{ for } t > t_N \tag{5}$$

where T_N is the final temperature after N jumps. In Fig. 2C we show how Eq. 5 predicts the output of a small sinusoidal temperature perturbation. The frequency of the perturbation is $2.3 \cdot 10^{-5}$ Hz, which is the inverse of the estimated equilibrium relaxation time of the sample at the reference temperature 164.6 K. The amplitude is 100 mK, i.e., within the linear limit of a

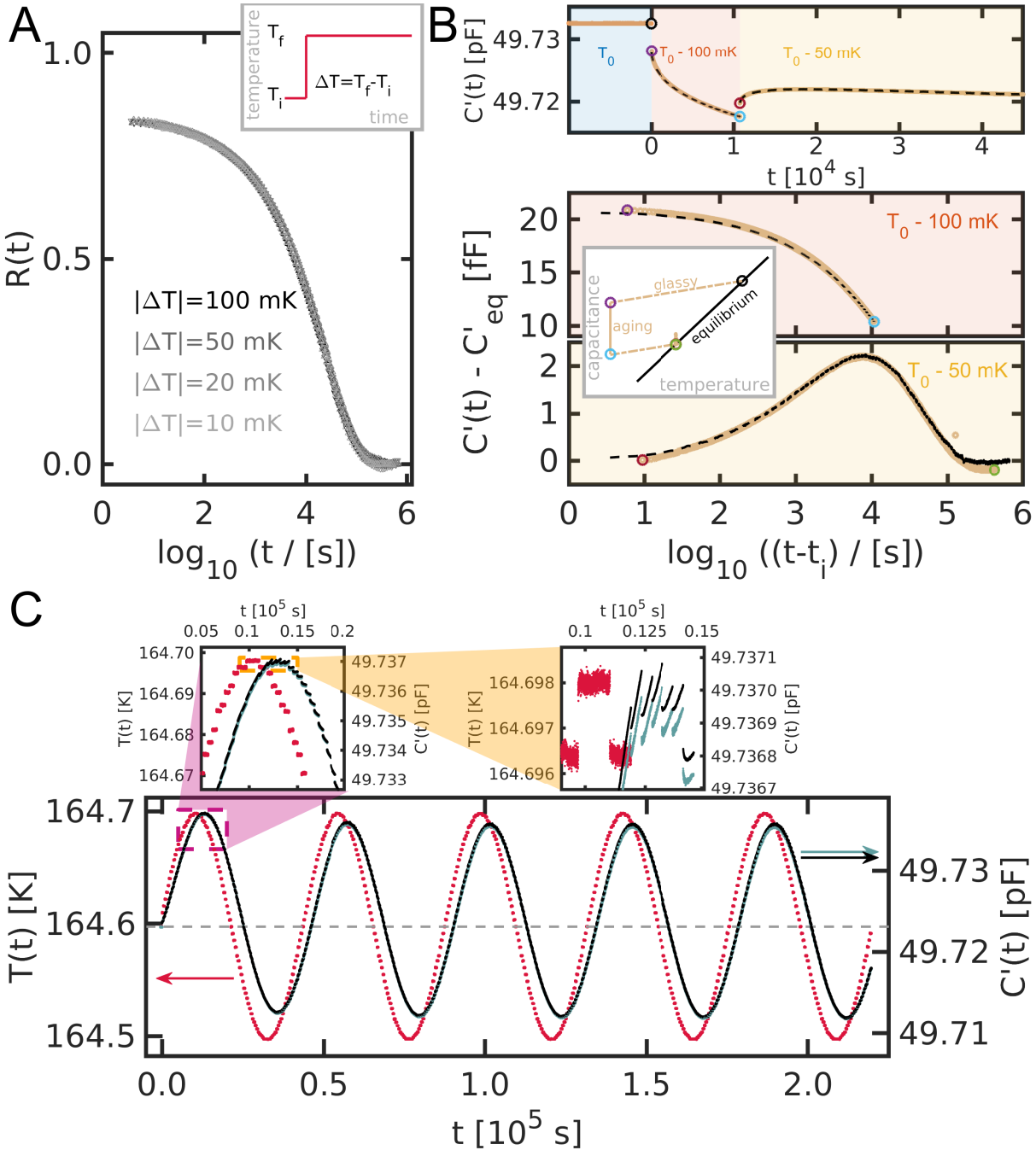

FIG. 2: Data for the real part of the capacitance, $C'(10\,\mathrm{kHz})$, from small-amplitude temperature modulation experiments on VEC along with predictions demonstrating that the response is linear. A Normalized relaxation function (Eq. 3) of single temperature jumps of amplitude 10 mK-100 mK around the reference temperature $T_0 = 164.6\ K$. All data collapse as predicted for linear relaxation. B Data from a small-amplitude temperature double jump starting at $T_0 = 164.6\ K$ and jumping first by -100 mK and then by +50 mK (colored curves) along with the prediction according to Eq. 4 (black dashed lines). The upper panel shows the full experiment on a linear time scale, the lower panel shows the data on a logarithmic time scale that sets the time of the beginning of each temperature jump to zero. The inset illustrates the protocol. C Sinusoidal small-amplitude temperature protocol (red points) and data (turquoise points). The prediction based on the linear-response formalism (Eq. 5) is shown as black points. Deviations between prediction and data can barely be discerned in the main figure, but can be seen in the zooms shown.

single jump. The prediction follows the data with a high accuracy, including both the transient behavior (seen, e.g., in a first peak that is higher than the second) and the phase shift. Tiny deviations between prediction and data can be seen in the inset, which also shows how the temperature protocol is composed of 2 mK temperature steps.

After establishing the linear aging limit and showing how linear temperature-jump data can be used to predict the response of other linear temperature protocols, we now turn to the main result of this paper, a proof of the existence of a material time for VEC. The radically new idea of the 1970s [3, 6] was that aging becomes linear when it is described in terms of the material time $\xi(t)$ instead of the laboratory time t. In addition one assumes so-called "time-aging-time-superposition", meaning that the spectral shape of $R_{\rm lin}$ is independent of the state of the sample. The consequence of these assumptions is that Eq. 1, Eq. 4, and Eq. 5 describe also nonlinear experiments simply by replacing the laboratory time with the material time, i.e.,

$$X(\xi) = \sum_{i=1}^{N} \Delta X_i R_{\rm lin}(\xi - \xi_i) + X_{\rm eq}(T_N) \text{ for } \xi > \xi_N \tag{6}$$

The material time is "measured" by a clock with a rate that reflects the state of the sample, and the nonlinearity of physical aging is a consequence of this fact [3, 6]. The material time may be thought of as analogous to the proper time in the theory of relativity, which is the time recorded on a clock following the observer. Although the origin of the material time is still somewhat of a mystery, the material-time concept is generally recognized to form the basis of a good description of physical aging involving relatively small temperature variations [4]. The very fundamental assumption of the formalism, however, that nonlinear aging phenomena can be predicted from the linear aging limit, has never been validated. In the following we do this by showing how the measured linear response determines the response to non-linear temperature protocols. This is done here for VEC and in the Supplementary Materials for NMEC.

Using Eq. 6 requires a connection between the laboratory time t and the material time ξ. This is obtained by introducing the time-dependent aging rate $\gamma(t)$ defined [3–8] by

$$\gamma(t) = d\xi(t)/dt. \tag{7}$$

In equilibrium, the aging rate is the relaxation rate $\gamma_{\rm eq}$ defined as the inverse of the equilibrium relaxation time. Thus a linear experiment can be considered the limiting case for which the aging rate is constant and the material time is proportional to the laboratory time, $\xi_{\rm lin}(t) = \gamma_{\rm eq} t$.

Different strategies have been used to estimate $\gamma(t)$ during aging, often via a fictive temperature [4, 22, 24]. We here adopt the simple single-parameter-aging ansatz according to which the aging rate is controlled by the measured quantity $X(t)$ itself as follows [37]

$$\log(\gamma(t)) - \log(\gamma_{\rm eq}(T)) = \Lambda(X(t) - X_{\rm eq}(T)). \tag{8}$$

Here $\gamma_{\rm eq}(T)$ and $X_{\rm eq}(T)$ are the equilibrium values of γ and X at the temperature T, and Λ is a proportionality constant that depends only on the substance and the monitored property X. It should be noted that Eq. 8 is arrived at by first-order Taylor expansions and can only be expected to apply for relatively small temperature variations.

The material-time description in Eq. 6, combined with Eq. 7 and Eq. 8, gives a unique prediction for $X(t)$ for any temperature protocol. Equation 6 predicts the value of $X(\xi)$ while Eqs. (7) and (8) connect the material and laboratory times by stretching or compressing the time-scale axis. The input needed for the prediction are $R_{\rm lin}(t)$ as determined in Fig. 2A, $\gamma_{\rm eq}(T)$, $X_{\rm eq}(T)$, and Λ. We have equilibrium measurements of $X_{\rm eq}(T)$ down to 163.6 K and have extrapolated values to lower temperatures (see the Supplementary Materials). The values used for $\gamma_{\rm eq}(T)$ are extrapolations from a fit of dielectric spectra, which down to 163.6 K and are shown to by proportional to the aging rates (see the Supplementary Materials). The parameter Λ is determined from sets of two nonlinear temperature jump experiments as described in Ref. 37 and the Supplementary Materials. Figure 3A shows $R(t)$ data from the nonlinear single-temperature jumps. It is seen that the short-time plateau of $R(t)$ for the different jumps do not coincide. This is due to a difference in the short-time relaxation deriving most likely from one or more beta relaxations. In order to predict the aging, we have adjusted for this difference in a manner where the short-time decay of $R(t)$ depends on both the initial and final temperatures (see the Supplementary Materials).

Figure 3 shows the main results of the paper: data from non-linear temperature protocols along with predictions based on the linear temperature-jump data. The nonlinear protocols mirror the linear protocols of Fig. 2. Figure 3A shows single temperature jumps, Fig. 3B shows a -2 K and +1 K double jump, and Fig. 3C shows a sinusoidal temperature modulation with amplitude 3 K and the same frequency as the linear sinusoidal protocol of Fig. 2.

The single jumps in Fig. 3A show the asymmetry of approach characteristic of nonlinear aging [10, 35]: "self-acceleration" of up jumps where the relaxation rate speeds up as equilibrium is reached and "self-retardation" of down jumps [8]. The material-time formalism captures well this asymmetry, and the measured data are predicted with a high accuracy for all down-jumps and for up-jumps up to 2 K. However, there is a significant deviation for the largest (3 K) up-jump and in the Supplementary Materials it is documented that deviations emerge already with a 2.5 K up-jump (for the NMEC data of the Supplementary Materials the formalism works well also for a 3 K up-jump). This shows the formalism breaks down for large amplitude up-jumps, a breakdown that sets in at different jump sizes depending on the sample. This may be caused by the sample reaching

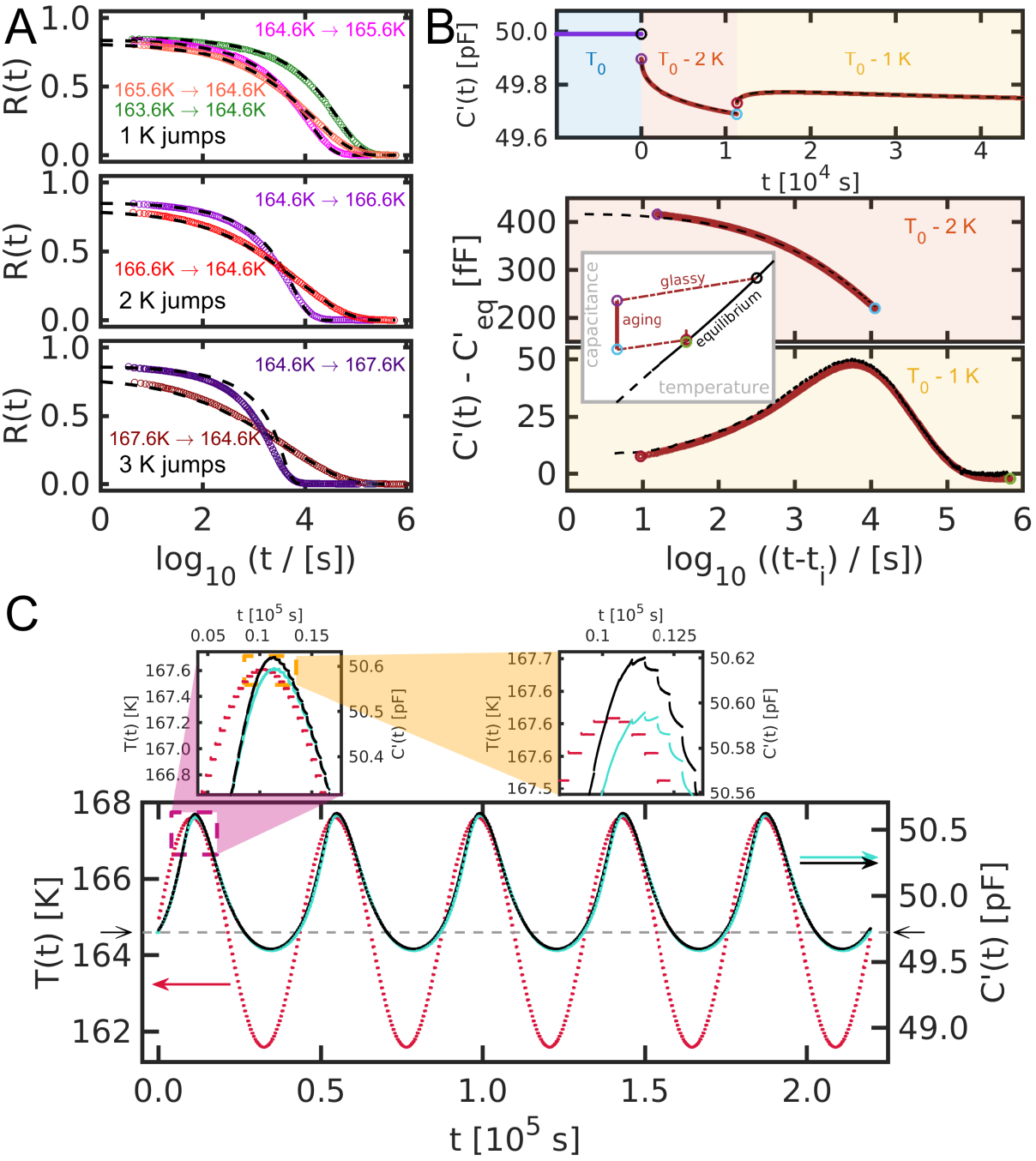

FIG. 3: Data from the real part of the capacitance, $C'(10\text{kHz})$, from large-amplitude temperature-modulation experiments on VEC along with predictions based on the measured linear response $R_{\text{lin}}(t)$ and the material time ansatz, i.e., Eq. 6 combined with Eq. 7 and Eq. 8. Colored curves are data and black dashed lines are predictions. A Normalized relaxation function (Eq. 3) of single temperature jumps with amplitudes ranging from 1 K to 3 K. B Data from a double jump starting at $T_0 = 167.6\ K$ and jumping by -2 K and +1 K (colored curves). The upper panel shows the full experiment on a linear time scale, the lower panel shows the data on a logarithmic time scale setting the time of the beginning of each temperature jump to zero. The inset illustrates the protocol. C Sinusoidal temperature protocol (red points) and data (turquoise points) shown together. The grey horizontal dashed line marks the equilibrium capacitance at the starting temperature 164.6 K. The prediction of the material-time formalism is shown as black points. The response is highly nonlinear, resulting in a non-sinusoidal curve that is far from symmetric around the horizontal dashed line marking the equilibrium value at the starting temperature. The deviations between prediction and data that can barely be discerned in the main figure are visible in the zooms shown above the main figure.

equilibrium through other mechanisms, possibly similar to what is seen in the case of very large up-jumps (30-70 K) performed on ultrastable vapor-deposited glasses where it has been shown that equilibrium is reached by heterogeneous growth of mobile domains [38].

The predictions agree well with the data of the non-linear double jumps shown in Fig. 3B, which demonstrates that the material-time formalism works well also in this situation. The data shown here are all from measurements in the temperature range where we have access to measured values of X_{eq}, γ_{eq}, and the fast contribution of $R(t)$. The parameter Λ is the same as for the single jumps and the test of the nonlinear double-jump prediction is therefore performed with no free parameters. In contrast, in the classical Ritland-Kovacs cross-over experiment the first down-jump goes deep into the glass state where the properties of the equilibrium liquid are not known. In the Supplementary Material we show data of a larger down jump (7 K); the predictions using extrapolated parameters demonstrate qualitatively good results although the formalism of course cannot predict the times scale of aging in the temperature regime where equilibrium cannot be reached.

Finally, Fig. 3C shows the response of the nonlinear sinusoidal temperature modulation along with the predictions. The lowest temperatures in the modulation are in a range where the parameters are extrapolated, and again there are no free parameters in the prediction. The nonlinearity is seen clearly as a significant asymmetry in the peak shape: when the temperature increases, there is a large response whereas the liquid responds much less to a decreased temperature. Note that the grey horizontal dashed line corresponds to the equilibrium capacitance at the starting temperature 164.6 K. This asymmetry is very well captured by the prediction. Deviations between prediction and data can be seen in the zoom in of the top of Fig. 3C and most likely related to the first-order nature of Eq. 8.

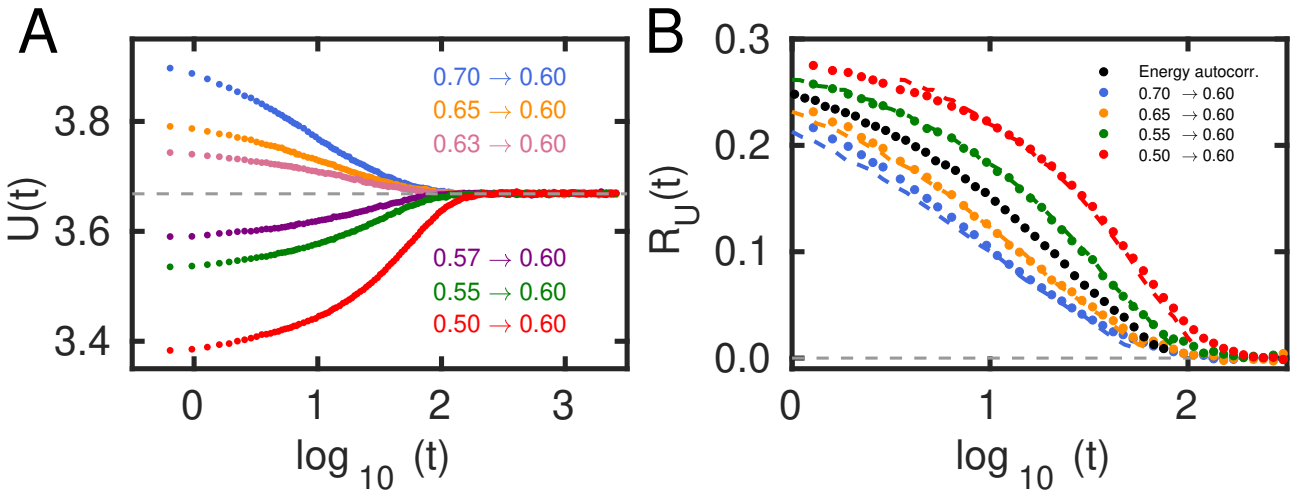

FIG. 4: Results from computer simulations of a binary model liquid monitoring the potential energy U. A shows data for six temperature jumps to the same temperature ($T = 0.60$ in rationalized units). B shows the normalized relaxation function, $R_U(t)$, of the thermal equilibrium potential-energy time-autocorrelation function at this temperature (black dots) and the predictions based on this for the temperature jumps (colored dashed curves). The data for the normalized relaxation functions based on A are shown as colored dots.

The results in Fig. 3 demonstrate that nonlinear physical-aging phenomena may be predicted from a knowledge of the linear limit of aging. While this limit is challenging to probe experimentally, it is conceptually important. First of all, it validates the central assumption of the material-time formalism. Secondly, linear-response theory is well established via the fluctuation-dissipation (FD) theorem that predicts the response from thermal fluctuations quantified via an equilibrium time-correlation function [39]. Our results therefore imply that nonlinear physical aging can now – at least in principle for relatively small jumps – be predicted from measurements of the equilibrium fluctuations, i.e., without perturbing the system at all. We have not yet attempted to do this experimentally, which is clearly a challenge, but end the paper by illustrating this possibility by presenting results from a computer simulation where thermal fluctuations are easily monitored.

The system studied is the binary Lennard-Jones mixture of Kob and Andersen [40], which in more than 20 years has been the standard model for computer simulations of glass-forming liquids. We simulated a system of 8000 particles. The quantity monitored is the potential energy U. Temperature-jump data are averaged over 1000 simulations to reduce the noise. Figure 4A shows results for jumps from six different temperatures to $T = 0.60$ (in rationalized units) plotted as a function of the logarithm of the time that has passed after each jump was initiated. The curves are quite different, showing that the jumps are large enough to be nonlinear.

The FD theorem implies that the linear response to an arbitrary small temperature variation is uniquely determined by the potential-energy time-autocorrelation function $\langle U(0)U(t)\rangle$ [41]. We evaluated this quantity at $T = 0.60$. Using the above single-

parameter material-time formalism we can then predict nonlinear temperature-jump results (Fig. 4B). The only free parameter of the fit is the parameter Λ of Eq. 8, which was determined from two jumps [37], here the two smallest ones. The colored dashed curves in B are the predictions for the normalized relaxation functions, while the full circles are the data corresponding to Fig. 4A; the black circles in the middle give the thermal-equilibrium time-autocorrelation function of the potential energy. Overall the predictions work well, demonstrating for the first time that nonlinear aging can be predicted from equilibrium fluctuations. The deviations for the two largest jumps are not surprising, given that these involve temperature changes of more than 15% for which Eq. 8 is likely to be inaccurate.

In this paper we have shown how nonlinear aging behavior can be predicted from the linear aging response, i.e., from the response to a very small temperature variation. This validates the central assumption of the material-time formalism for the first time. At the same time, it is clear that this formalism has limitations. Thus the largest up jump (3 K) is not well predicted (Fig. 3A, lower panel). This suggests that there are two regimes of non-linear aging: An intermediate nonlinear regime where the relaxation time varies at most a few decades and the material-time concept describes the situation well, and a strongly nonlinear regime where the formalism breaks down and a new theoretical approach is needed. We speculate that even large temperature down jumps may well fall into the intermediate regime because the system here thermalizes gradually; this is in contrast to large up jumps which are known to result in heterogeneous states very far from equilibrium [38]. Along this line of thinking, the standard glass transition resulting from a continuous cooling is likely to be described well by the material-time formalism, i.e., is intermediate nonlinear because the freezing takes place over a narrow range of temperatures and thus effectively gives the same situation as a in a large down-jump.

In regard to the intermediate regime of physical aging, the implications of our findings are profound both for the understanding of aging in application and for the theoretical interpretation of the aging dynamics. By reference to the FD theorem, the consequence is that the properties governing the nonlinear physical aging of a system far from equilibrium is embedded in the thermal equilibrium fluctuations and can be predicted from these. This means that there is no fundamental difference between the nonlinear and the linear aging responses. In other words, the both classical and active research on characterizing and understanding the spectral shape of linear response and correlation functions experimentally [42, 43], as well as theoretically [44], is intimately linked to the understanding of physical aging.

ACKNOWLEDGMENTS

This work was supported by the VILLUM Foundation's *Matter* grant (No. 16515).

[1] O. Mazurin, "Relaxation phenomena in glass," J. Non-Cryst. Solids, vol. 25, pp. 129–169, 1977.
[2] L. C. E. Struik, Physical Aging in Amorphous Polymers and Other Materials. Elsevier, Amsterdam, 1978.
[3] A. J. Kovacs, J. J. Aklonis, J. M. Hutchinson, and A. R. Ramos, "Isobaric Volume and Enthalpy Recovery of Glasses. II. A Transparent Multiparameter Theory," J. Polym. Sci. Polym. Phys., vol. 17, no. 7, pp. 1097–1162, 1979.
[4] G. W. Scherer, Relaxation in Glass and Composites. New York: Wiley, 1986.
[5] I. M. Hodge, "Physical aging in polymer glasses," Science, vol. 267, pp. 1945–1947, 1995.
[6] O. S. Narayanaswamy, "A model of structural relaxation in glass," J. Am. Ceram. Soc., vol. 54, p. 491, 1971.
[7] M. Micoulaut, "Relaxation and physical aging in network glasses: a review," Rep. Prog. Phys., vol. 79, p. 066504, 2016.
[8] D. Cangialosi, V. M. Boucher, A. Alegria, and J. Colmenero, "Physical aging in polymers and polymer nanocomposites: recent results and open questions," Soft Matter, vol. 9, pp. 8619–8630, 2013.
[9] C. B. Roth, ed., Polymer Glasses. CRC Press (Boca Raton, FL, USA), 2017.
[10] G. B. McKenna and S. L. Simon, "50th anniversary perspective: Challenges in the dynamics and kinetics of glass-forming polymers," Macromolecules, vol. 50, pp. 6333–6361, 2017.
[11] S. V. Ketov, Y. H. Sun, S. Nachum, Z. Lu, A. Checchi, A. R. Beraldin, H. Y. Bai, W. H. Wang, D. V. Louzguine-Luzgin, M. A. Carpenter, and A. L. Greer, "Rejuvenation of metallic glasses by non-affine thermal strain," Nature, vol. 524, pp. 200–203, 2015.
[12] B. Ruta, E. Pineda, and Z. Evenson, "Relaxation processes and physical aging in metallic glasses," J. Phys.: Condens. Mat., vol. 29, p. 503002, 2017.
[13] J. Ketkaew, R. Yamada, H. Wang, D. Kuldinow, B. S. Schroers, W. Dmowski, T. Egami, and J. Schroers, "The effect of thermal cycling on the fracture toughness of metallic glasses," Acta Mater., vol. 184, pp. 100–108, 2020.
[14] S. Vyazovkin and I. Dranca, "Effect of physical aging on nucleation of amorphous indomethacin," J. Phys. Chem. B, vol. 111, pp. 7283–7287, 2007.
[15] F. Bonacci, X. Chateau, E. M. Furst, J. Fusier, J. Goyon, and A. Lemaitre, "Contact and macroscopic ageing in colloidal suspensions," Nat. Mater., vol. 19, pp. 775–780, 2020.
[16] J. C. Mauro, "Presentation at "Unifying Concepts in Glass Physics. VI." Aspen, Colorado ," February 2015.
[17] E. Andersen, R. Mikkelsen, S. Kristiansen, and M. Hinge, "Accelerated physical ageing of poly(1,4-cyclohexylenedimethylene-co-2,2,4,4-tetramethyl-1,3-cyclobutanediol terephthalate)," RSC Adv., vol. 9, pp. 14209–14219, 2019.

[18] J. Fonseca, T. Gong, L. Jiao, and H.-L. Jiang, "Metal-organic frameworks (mofs) beyond crystallinity: amorphous mofs, mof liquids and mof glasses," J. Mater. Chem. A, vol. 9, pp. 10562–10611, 2021.

[19] S. Zhao, Z. Li, C. Zhu, W. Yang, Z. Zhang, D. E. J. Armstrong, P. S. Grant, R. O. Ritchie, and M. A. Meyers, "Amorphization in extreme deformation of the crmnfeconi high-entropy alloy," Science Advances, vol. 7, no. 5, 2021.

[20] F. Arceri, F. P. Landes, L. Berthier, and G. Biroli, "Glasses and aging: A statistical mechanics perspective," arXiv:2006.09725, 2020.

[21] L. F. Cugliandolo and J. Kurchan, "On the out-of-equilibrium relaxation of the Sherrington-Kirkpatrick model," J. Phys. A: Math. Gen., vol. 27, no. 17, pp. 5749–5772, 1994.

[22] A. Q. Tool, "Relation between inelastic deformability and thermal expansion of glass in its annealing range," J. Am. Ceram. Soc., vol. 29, no. 9, pp. 240–253, 1946.

[23] J. C. Dyre, "Narayanaswamy's 1971 aging theory and material time," J. Chem. Phys., vol. 143, no. 11, p. 114507, 2015.

[24] G. B. McKenna, "Looking at the glass transition: Challenges of extreme time scales and other interesting problems," Rubber Chem. Technol., vol. 93, pp. 79–120, 2020.

[25] T. Hecksher, N. B. Olsen, K. Niss, and J. C. Dyre, "Physical aging of molecular glasses studied by a device allowing for rapid thermal equilibration," J. Chem. Phys., vol. 133, p. 174514, 2010.

[26] B. Igarashi, T. Christensen, E. H. Larsen, N. B. Olsen, I. H. Pedersen, T. Rasmussen, and J. C. Dyre, "A cryostat and temperature control system optimized for measuring relaxations of glass-forming liquids," Rev. Sci. Instrum., vol. 79, p. 045105, 2008.

[27] K. Niss, D. Gundermann, T. Christensen, and J. C. Dyre, "Dynamic thermal expansivity of liquids near the glass transition," Phys. Rev. E, vol. 85, p. 041501, 2012.

[28] K. Niss, "Mapping isobaric aging onto the equilibrium phase diagram," Phys. Rev. Lett., vol. 119, p. 115703, 2017.

[29] K. Niss, J. C. Dyre, and T. Hecksher, "Long-time structural relaxation of glass-forming liquids: Simple or stretched exponential?," J. Chem. Phys., vol. 152, p. 041103, 2020.

[30] P. Lunkenheimer, R. Wehn, U. Schneider, and A. Loidl, "Glassy aging dynamics," Phys. Rev. Lett., vol. 95, p. 055702, 2005.

[31] R. Richert, "Supercooled liquids and glasses by dielectric relaxation spectroscopy," Adv. Chem. Phys., vol. 156, pp. 101–195, 2015.

[32] P. Lunkenheimer, S. Kastner, M. Köhler, and A. Loidl, "Temperature development of glassy α-relaxation dynamics determined by broadband dielectric spectroscopy," Phys. Rev. E, vol. 81, p. 051504, May 2010.

[33] M. Paluch, Z. Wojnarowska, and S. Hensel-Bielowka, "Heterogeneous dynamics of prototypical ionic glass ckn monitored by physical aging," Phys. Rev. Lett., vol. 110, p. 015702, Jan 2013.

[34] B. Jakobsen, K. Niss, and N. B. Olsen, "Dielectric and shear mechanical alpha and beta relaxations in seven glass-forming liquids," J. Chem. Phys., vol. 123, p. 234511, 2005.

[35] A. J. Kovacs, "Transition vitreuse dans les polymeres amorphes. Etude phenomenologique," Fortschr. Hochpolym.-Forsch, vol. 3, p. 394, 1963.

[36] T. Hecksher, N. B. Olsen, and J. C. Dyre, "Fast contribution to the activation energy of a glass-forming liquid," Proc. Natl. Acad. Sci., vol. 116, pp. 16736–16741, 2019.

[37] T. Hecksher, N. B. Olsen, and J. C. Dyre, "Communication: Direct tests of single-parameter aging," J. Chem. Phys., vol. 142, p. 241103, 2015.

[38] A. Sepúlveda, M. Tylinski, A. Guiseppi-Elie, R. Richert, and M. D. Ediger, "Role of fragility in the formation of highly stable organic glasses," Phys. Rev. Lett., vol. 113, p. 045901, 2014.

[39] L. E. Reichl, A Modern Course in Statistical Physics. Wiley-VCH, 4th edition ed., 2016.

[40] W. Kob and H. C. Andersen, "Testing Mode-Coupling Theory for a Supercooled Binary Lennard-Jones Mixture I: The van Hove Correlation Function," Phys. Rev. E, vol. 51, pp. 4626–4641, 1995.

[41] J. K. Nielsen and J. C. Dyre, "Fluctuation-dissipation theorem for frequency-dependent specific heat," Phys. Rev. B, vol. 54, pp. 15754–15761, 1996.

[42] T. Körber, R. Stäglich, C. Gainaru, R. Böhmer, and E. A. Rössler, "Systematic differences in the relaxation stretching of polar molecular liquids probed by dielectric vs magnetic resonance and photon correlation spectroscopy," J. Chem. Phys., vol. 153, no. 12, p. 124510, 2020.

[43] F. Pabst, J. Gabriel, T. Böhmer, P. Weigl, A. Helbling, P. Richter, T. Zourchang, T. Walther, and B. T., "Generic structural relaxation in supercooled liquids," J. Phys. Chem. Lett., vol. 12,14, no. 3685–3690, 2021.

[44] B. Guiselin, C. Scalliet, and L. Berthier, "Microscopic origin of excess wings in relaxation spectra of deeply supercooled liquids," arXiv:2103.01569 [cond-mat.soft], 2021.

[45] B. Igarashi, T. Christensen, E. H. Larsen, N. B. Olsen, I. H. Pedersen, T. Rasmussen, and J. C. Dyre, "An impedance-measurement setup optimized for measuring relaxations of glass-forming liquids," Review of Scientific Instruments, vol. 79, no. 4, p. 045106, 2008.

[46] S. Nosé, "A unified formulation of the constant temperature molecular dynamics methods," The Journal of Chemical Physics, vol. 81, no. 1, pp. 511–519, 1984.

[47] N. P. Bailey, T. S. Ingebrigtsen, J. S. Hansen, A. A. Veldhorst, L. Bøhling, C. A. Lemarchand, A. E. Olsen, A. K. Bacher, L. Costigliola, U. R. Pedersen, et al., "RUMD: A general purpose molecular dynamics package optimized to utilize GPU hardware down to a few thousand particles," SciPost Phys, vol. 3, no. 6, p. 038, 2017.

SUPPLEMENTARY INFORMATION

Here follows supplementary information and figures complementing the data presented in the main publication. The data is organized in three sections. The first two present details on the experiments: Sec. A contains data on 4-vinyl-1,3-dioxolan-2-one (VEC), while Sec. B gives a brief overview on data on N-methyl-ε-caprolactam (NMEC). In Sec. C details to the computer simulations are given.

Supplementary Information A: VEC

1. Details on the data set measured on VEC

This section contains

a) spectra of the storage and loss dielectric permittivity measured by dielectric spectroscopy

b) details on temperature control

c) data-set of the loss capacitance

d) comparisons of the experimental response (storage part of capacitance) with predictions for single and double-jump temperature protocols in the linear ($\Delta T \leq 100$ mK) and nonlinear ($\Delta T > 100$ mK) regime

a. Spectra of storage and loss dielectric permittivity for VEC

All data shown for VEC were measured on the same sample.The sample material was inserted into a parallel-plate capacitor with a plate distance of 50 µm and a geometric capacitance of $C_{geo} = 16.2$ pF. This sample was quenched to $T_{cryo} = 163$ K by insertion into the pre-cooled cryostat and was hold at that temperature for 60 h. Then the spectra presented in Fig. S1 were measured while tracking the temperature-specific voltage of the micro-regulator.

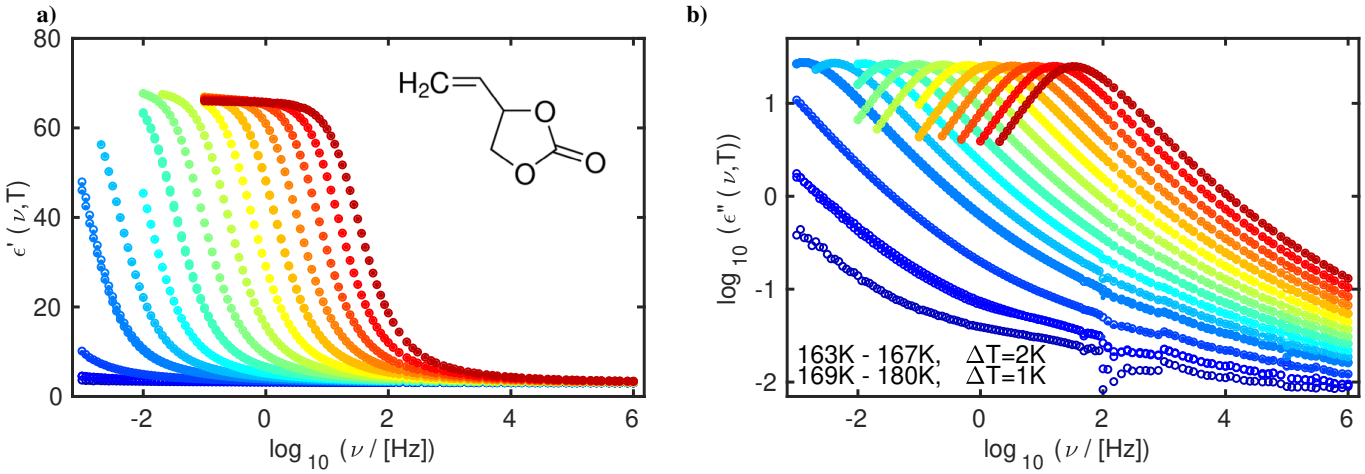

FIG. S1: Dielectric spectra for VEC. (a) Storage and (b) loss dielectric permittivity, $\varepsilon'(\nu)$ and ε"(ν), as functions of frequency measured by a high-precision custom-built frequency generator and a commercial LCR meter in a temperature range from 163 K to 180 K. The inset in panel (b) depicts the skeletal formula of VEC.

b. Temperature control

The temperature-control of the micro-regulator was calibrated with the temperature-specific microregulator voltage tracked during the measurements of spectra in the temperature range between 163 K and 180 K. Then the cryostat-controlled temperature was adjusted to $T_{cryo} = 164$ K and the micro-regulator was activated and set to $T = T_{MR} = 164.5$ K. While the sample environmet (cryostat) is held at T_{cryo}, the microregulator is now in control of the exact sample temperature. Details on the microregulator

setup are shown in Fig. S2. The regulation behavior of the microregulator can be tuned to ensure fast temperature equilibration, which is achieved after ca. 4 s for all temperature jumps performed on VEC. The microregulator also ensures high temperature stability, which is better than 1 mK.

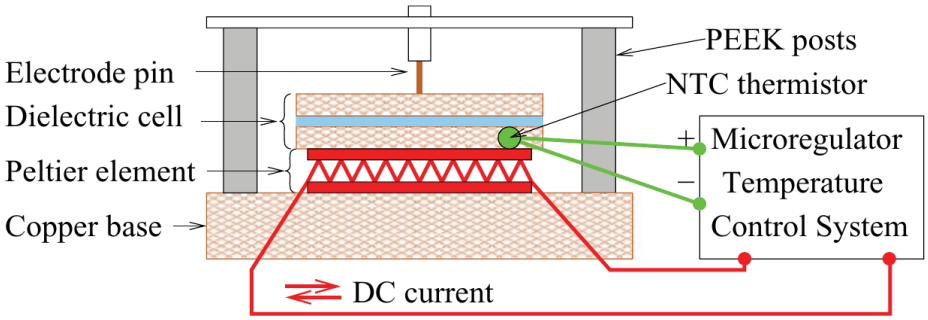

FIG. S2: Schematic drawing of capacitor (dielectric cell) and microregulator which is mounted in the main cryostat[25]. The liquid is inserted into the 50 µm gap between the disks of the dielectric cell. The Peltier element heats or cools the sample, depending on the direction of the electrical current powering the element. Details of the cryostat setup and the microreglator are described in Refs. 26 and 45.

c. Overview on loss-capacitance data

The dielectric response was measured with an Andeen-Hagerling ultra-precision capacitance bridge (model 2700A): the capacitance, C, and the dielectric loss, $\tan\delta$, were tracked at a frequency of $\nu = 10$ Hz.
Individual temperature jumps with amplitudes from $\Delta T = 2$ mK up to 3.5 K were initiated, as well as double-jump protocols with $\Delta T_1 = +100$ mK, -100 mK, -1 K, -2 K or -7 K and $\Delta T_2 = -\Delta T_1/2$, and multi-jump temperature protocols resembling an overall sinusoidal temperature variation with an amplitude of the sine of 100 mK or 3 K. An overview of the temperature protocol is given in Fig. S3 together with the corresponding loss capacitance.
The single temperature jumps of the loss capacitance are plotted in Fig. S4 as functions of the logarithm of the time that has passed since the initiation of the jump, $t - t_i$. To visualize the linearity of the jumps from Fig S4b), the normalized response function,

$$R_X(t) = \frac{X(t) - X_{eq}(T_f)}{X_{eq}(T_i) - X_{eq}(T_f)} = \frac{\Delta X(t)}{\Delta X}, \tag{s1}$$

is plotted in Fig. S5. The collapse of the data of all jumps with temperature amplitudes below 100 mK indicates the linear reponse regime at the given experimental accuracy. As jumps of 2 mK show a considerably lower signal-to-noise ratio as the setup is pushed closer to its limit in temperature control, only jumps with $\Delta T \geq 10$ mK are depicted here.

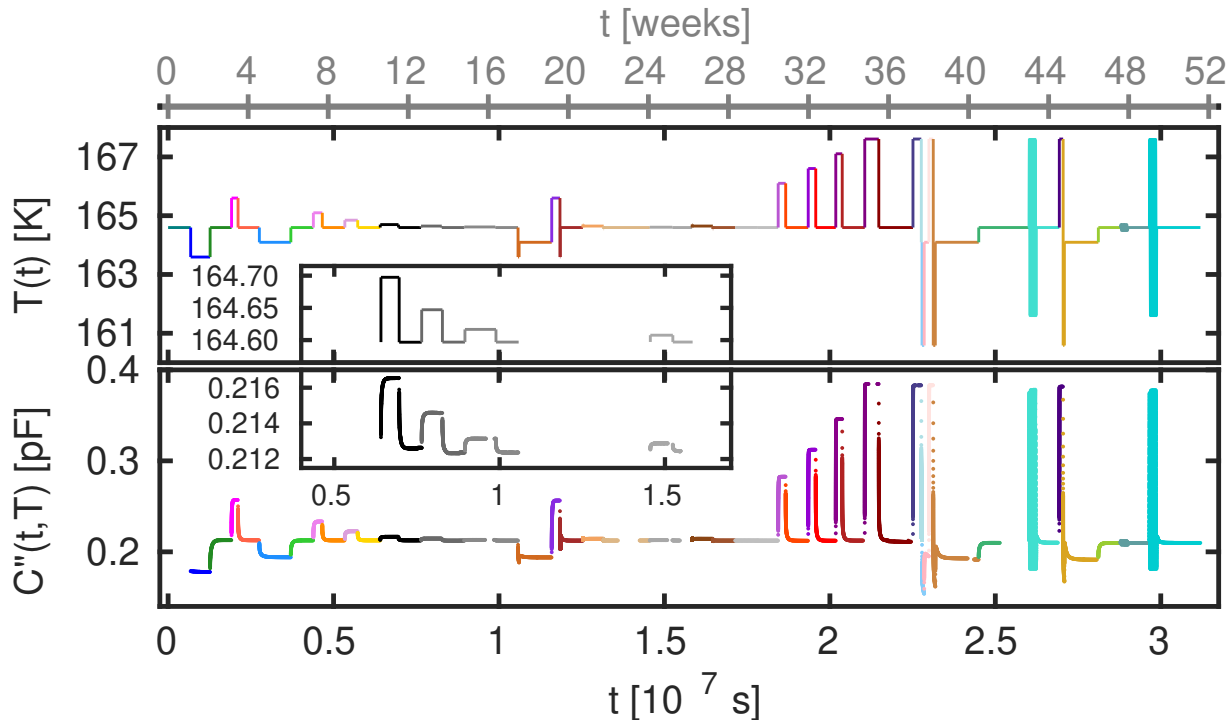

FIG. S3: Overview on the temperature protocol of consecutive physical-aging experiments realized by temperature jumps facilitated by an NTC thermistor regulated Peltier element around T_{ref} =164.6 K, and the loss capacitance, $C''(\nu = 10\,\text{kHz})$, as functions of time in seconds on the lower and weeks on the upper x-axis. Note that nonlinear aging data is colored while linear data is depicted on grey scale. The insets show single jumps with temperature amplitudes of 100 mK or less with a zoom on the y-axes.

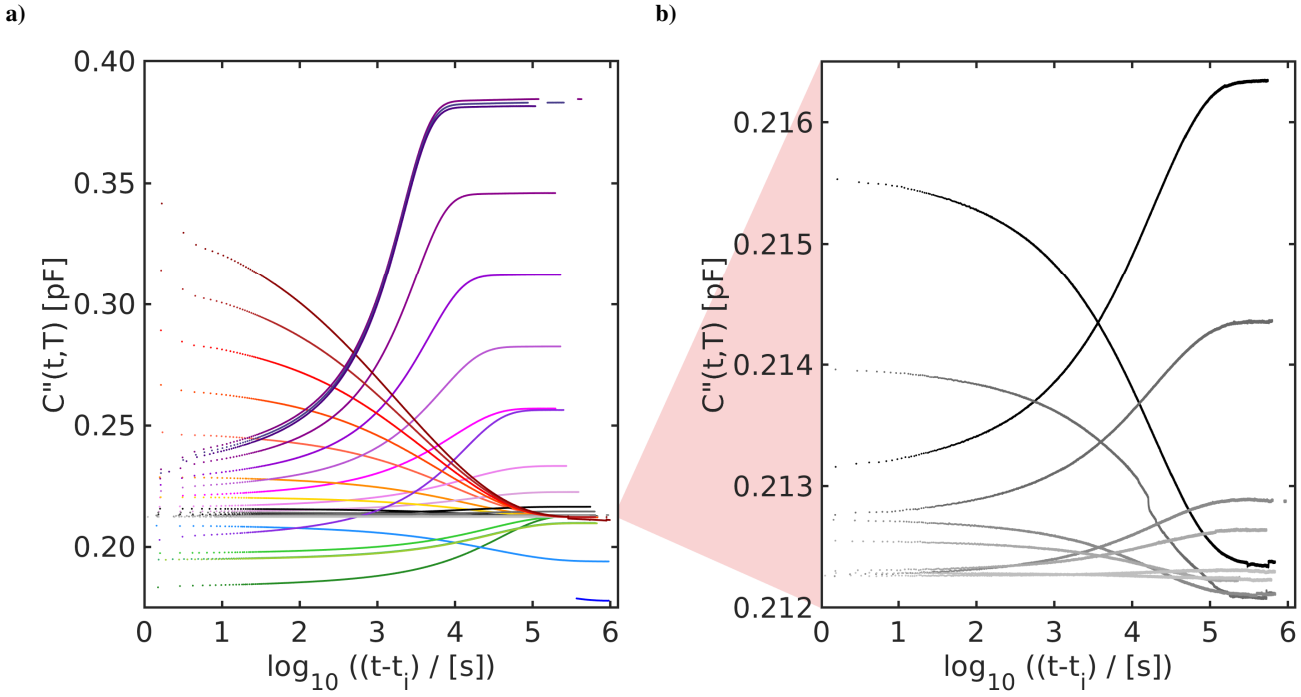

FIG. S4: Loss capacitance data, C"$(\nu = 10\,\text{kHz})$, plotted as functions of the logarithm of the time that has passed since the initiation of a jump at $t = t_i$. **a)** depicts data of all single temperature jumps and **b)** is a zoom on jumps of 2 mK to 100 mK temperature amplitude.

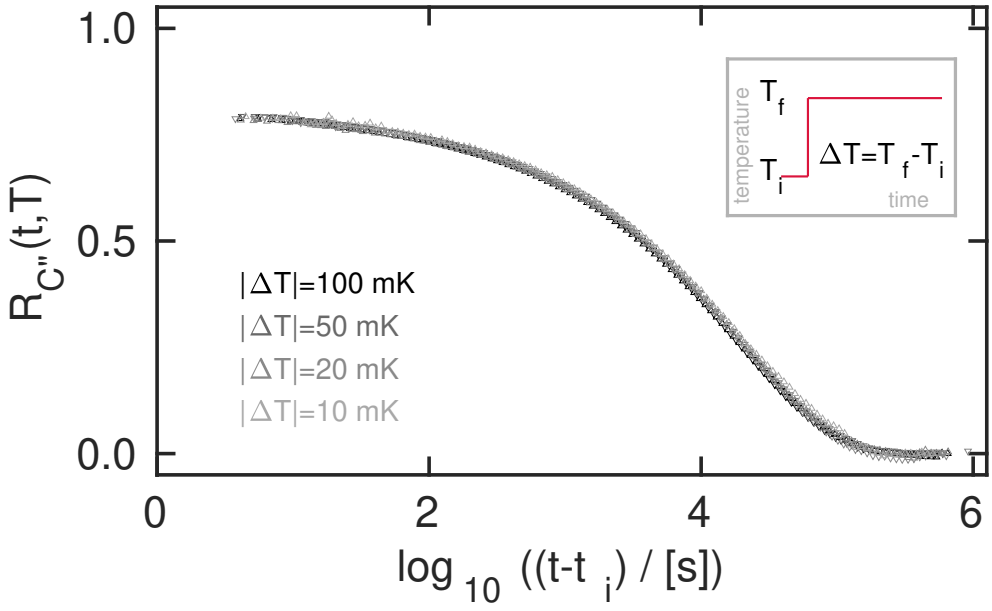

FIG. S5: Normalized relaxation function for loss part of capacitance data, $R_{C''}$, for single temperature jumps with amplitudes between 10 mK and 100 mK as functions of the logarithm of the time that has elapsed since the initiation of a jump at $t = t_i$.

d. Comparison of experimental data and predictions

In Fig. S6, experimental data and predictions are plotted following double-jump temperature protocols in the linear regime. One of the realizations in a) is included in the main manuscript, and the accurate match with the second realization gives a convincing confirmation of the achieved results. The double-jumps in b) follow an inverted Kovacs protocol, starting with an up-jump that is followed by a down-jump in temperature.

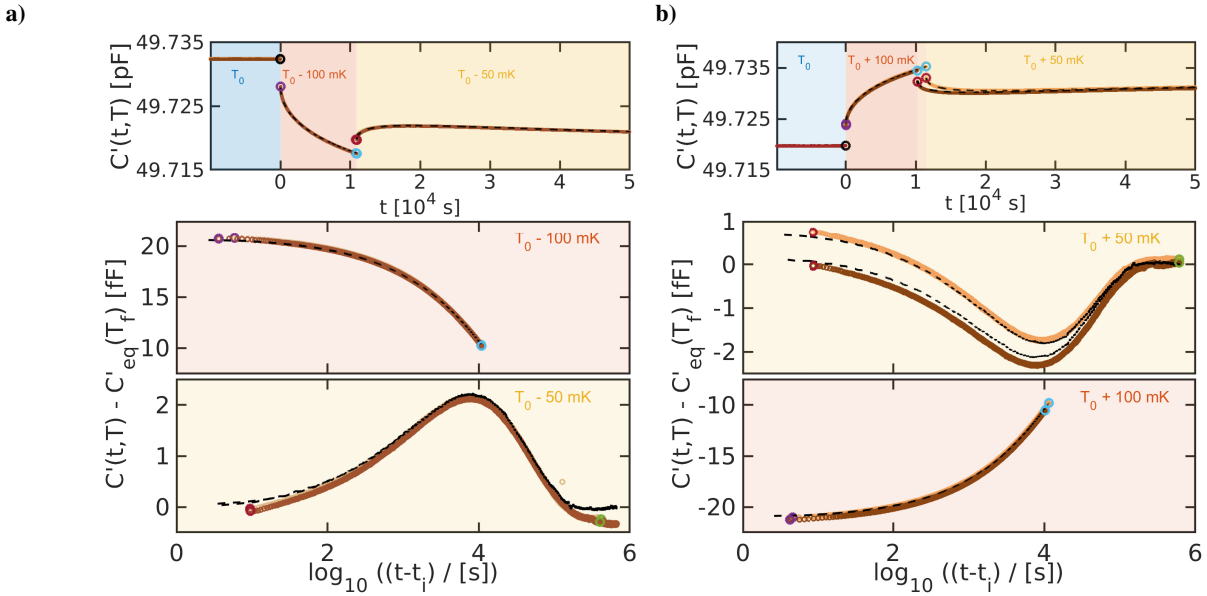

FIG. S6: Experimental data and predictions of linear double jumps on VEC involving temperature jumps of **a)** ΔT_1 =-100 mK and ΔT_2 =+50 mK and **b)** ΔT_1 =+100 mK and ΔT_2 =-50 mK for two realizations each. Upper panels show data plotted against linear time, middle and lower panels depict data as functions of the logarithm of the time that has elapse since the initiation of a jump at $t = t_i$. No corrections were made to yield the match between experimental data and prediction.

Note that the predictions capture the details of the responses with very high accuracy: While the second jump is initiated at precisely the same point for the two realizations in Fig. S6a), a difference in the initiation of the second jump of the two realizations shown in Fig. S6b) is observed. This leads to different levels in the short-time response at $T = T_0$+50 mK, which are reflected with high accuracy by the predictions.

The predictions and experimental responses to single temperature jumps with amplitudes larger than 100 mK, i.e. nonlinear individual jumps, are plotted in Fig. S7. In addition to the data of the main manuscript, three additional jump amplitudes are presented here: ΔT =0.5 K, ΔT =1.5 K, and ΔT =2.5 K. Note that the details of the aging responses are captured very accurately for all down-jumps, and for up-jumps with $\Delta T \leq$1 K, while the predictions show more and more pronounced signs of deviation from experimental data for larger up-jumps. A possible reason for this observation is a deviation from the aging behavior as assumed by the applied aging formalism. One possible scenario that matches the observed behavior is the initiation of a heterogeneous growth process as observed for very larger temperature up-jumps for ultrastable vapor-deposited glasses.

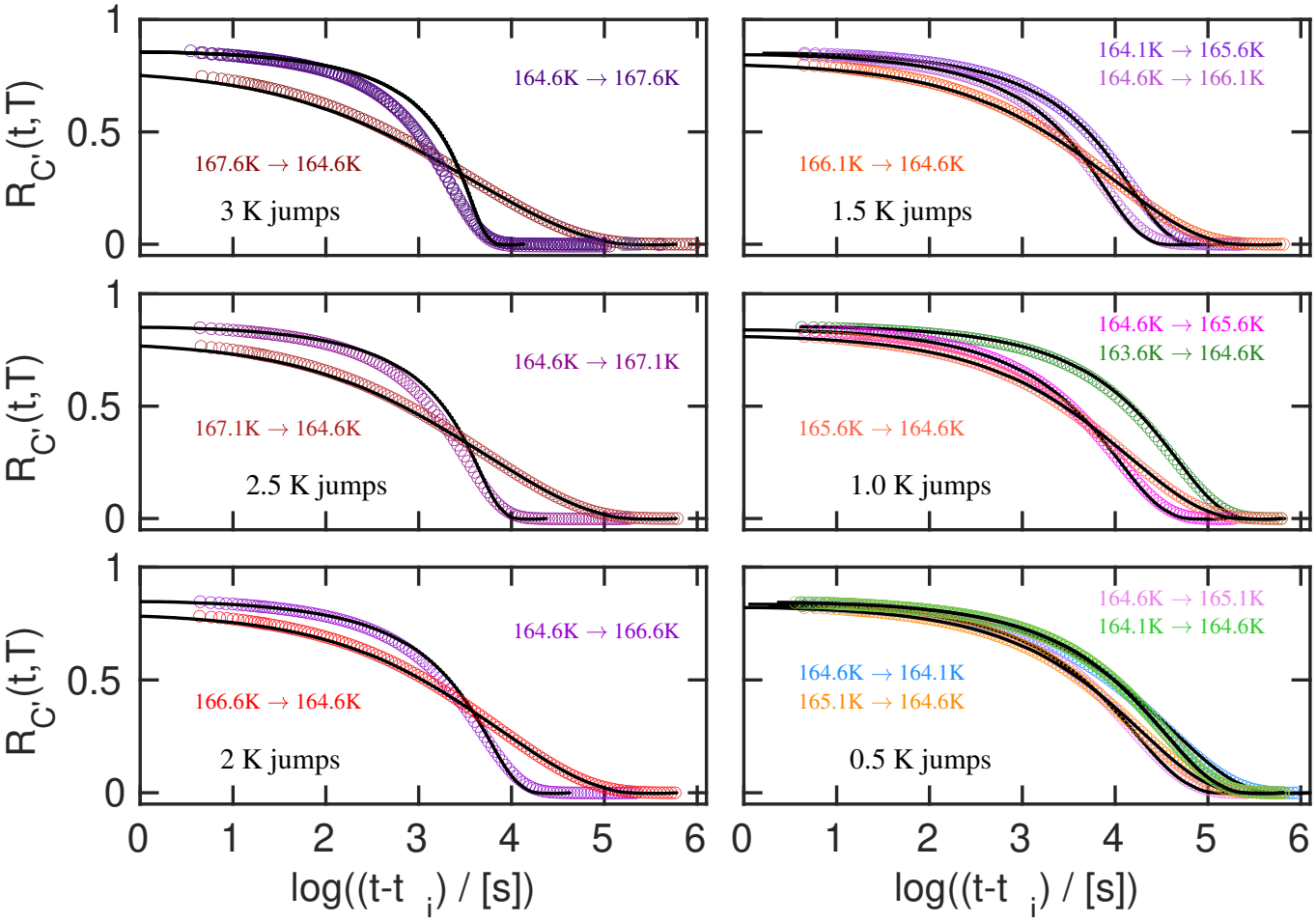

FIG. S7: Normalized response function based on measured storage capacitance and predictions of nonlinear individual jumps on VEC involving temperature jumps between 0.5 K and 3 K.

In Fig. S8, experimental data and predictions are plotted following double-jump temperature protocols in the nonlinear regime. In addition to the nonlinear double-jump that is included in the main manuscript (see Fig. S8), two more nonlinear double-jumps are presented here which have temperature amplitudes of ΔT_1 =1 K in a) and ΔT_1 =7 K in c). Panels a) to c) show experimental data and predictions without any corrections.
From these three nonlinear double-jumps, only the 7 K double-jump exceeds the temperature regime for which equilibrium-data can be interpolated, so that its predicitons are based on extrapolations far (3 K) below known equilibrium values. Thus it is not surprising that the prediction for the 7 K double-jump is deviating slightly from the experimental data. To check under which parameter-conditions predictions and experimental data coincide, we varied both the initial plateau of the second jump and the clock rate of the initial jump after making a minor adjustment of the overall data by shifting it by -8.1 fF to match zero in the long-time limit of the second jump. The outcome is shown in Fig. S8d). The glassy contribution of the second jump was

forced to match the data by multiplying the extrapolated parameter by 1.3 (visualized as grey diamond in Fig. S12). For the extrapolation of the clock rate the Avramov-function was applied instead of the Vogel-Fulcher-Tammann (VFT) extrapolation, corresponding to a factor of 1.5 on the VFT-extrapolation (visualized as black circle in Fig. S16). See Sec. A 2 for details for inter- and extrapolations of response-related parameters.

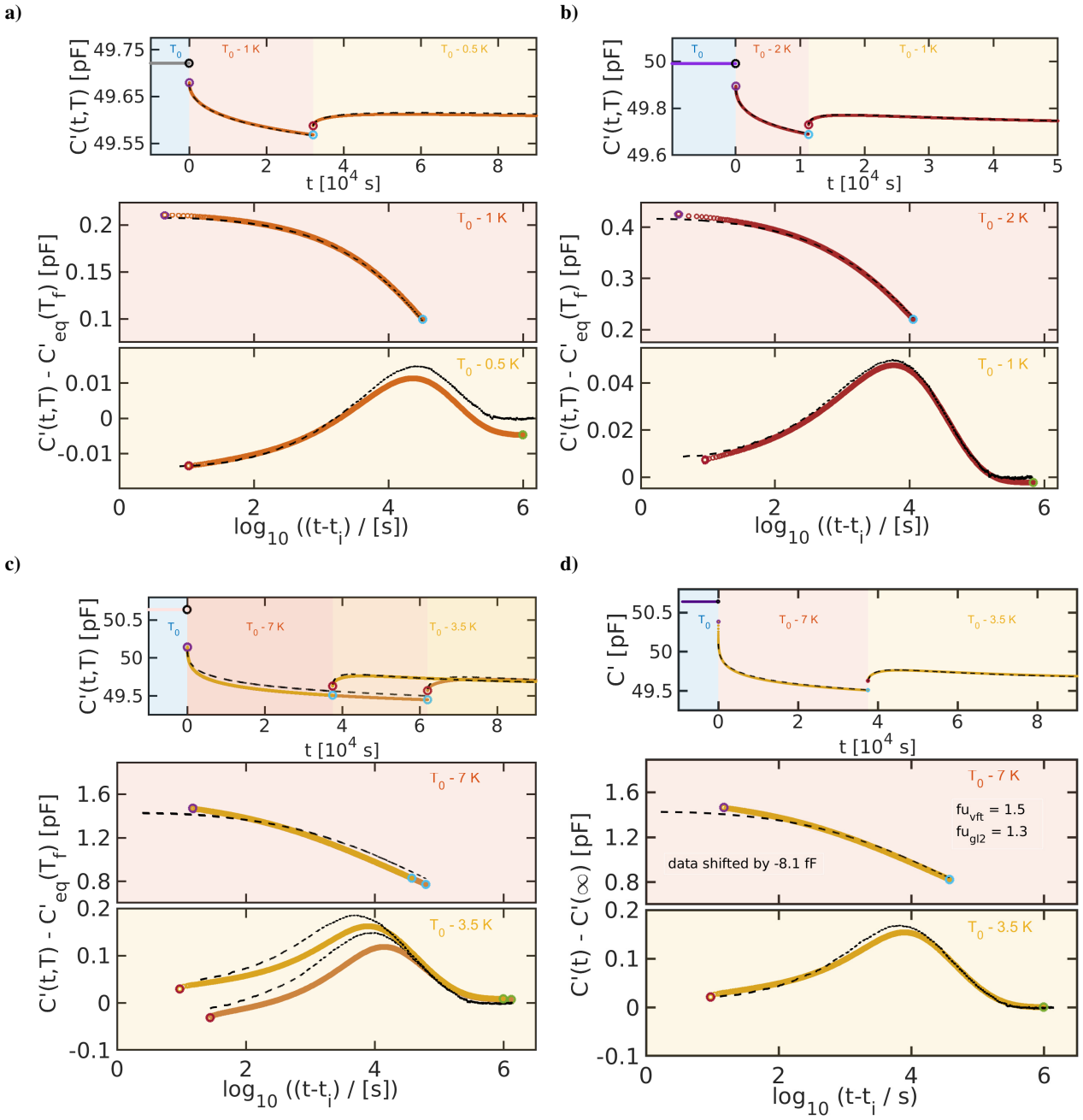

FIG. S8: Experimental data and predictions of nonlinear double jumps on VEC involving temperture jumps of **a)** ΔT_1 =-1 K and ΔT_2 =+0.5 K, **b)** ΔT_1 =-2 K and ΔT_2 =+1 K and **c)** ΔT_1 =-7 K and ΔT_2 =+3.5 K for two realizations. The predictions are based on inter- and extrapolation of the glassy contribution X_{gl}, the equilibrium response X_{eq}, Λ, and the equilibrium clock rate γ_{eq} . Note that for the predictions of the double jump with ΔT_1 =-7 K shwon in panel c) the afore-mentioned quantities had to be extrapolated, while the predictions of double-jumps in a) and b) are based on interpolations. For more details on how predictions are derived, see section A 4 b. No corrections were applied to yield the predictions shown in panels a) to c). In panel d) the data was shifted by -8.1 fF to match zero in the long-time limit of the second jump, and corrections for the clock rate and the glassy contribution of the second jump were applied.

2. Evaluation of response-specific parameters

This section covers:

a) details on the drift correction

b) equilibrium values of the measured quantity, X_{eq}

c) glassy contribution to the normalized response funciton, R_X^{gl}

d) equilibrium values of the relaxation rate, γ_{eq}

a. details on drift correction

The measured capacitance at constant temperature shows, even though the sample is equilibrated regarding physical aging, a small but steady decline (see Fig. S9). This time-dependent decline is termed "drift" in the context of this work and is described and analyzed in detail in this section.
The data is corrected for the drift by subtraction of a linearized contribution of the drift, which is either determined on the basis of individual jumps or sets of jumps specified as loops as described in the following.

individual drift correction

For each jump that is assumed to have achieved the equilibrium state (i.e. individual jumps, second part of double-jumps), a final 'linear-like' region in the long-time regime of the data was manually determined, typically involving ca. 10^4 data points. From a linear regression of these intervals following

$$X(t) = r_1 \times time + r_2, \tag{s2}$$

the drift is identified as the slope r_1 for the storage and loss response, respectively.

loop-wise drift correction

As for the individual drift correction, the 'linear-like' region in the long-time regime was manually determined for jumps that are assumed to have achieved equilibrium. For the loop-wise drift correction, subsequent jumps of same temperature amplitude ΔT are regarded as a 'loop' or set of jumps, typically consisting of four consecutive jumps (from or to T_b by $\pm\Delta T$) or two consecutive jumps (from or to T_b by $+\Delta T$). The drift is determined from the slope s_1 of linear fits based on

$$\begin{pmatrix} X_{j1}(t) \\ X_{j2}(t) \\ X_{j3}(t) \\ X_{j4}(t) \end{pmatrix} = s_1 \times \begin{pmatrix} t_{j1} + s_2 \\ t_{j2} + s_3 \\ t_{j3} + s_4 \\ t_{j4} + s_5 \end{pmatrix}. \tag{s3}$$

for the response of the storage and loss component, respectively. Here we assume that all jumps of a loop, which have different response 'offsets' s_2 to s_5, share the same slope s_1.

Based on the individual correction and the loop-wise correction, the raw time-dependent response-data is corrected by substracting the cummulated drift-contribution since the initialization of the experiment. The resulting corrected data-sets are shown in Fig. S10a) for the storage response and in Fig. S10b) for the loss response.
In the following sections A 2 b to A 2 d it is demonstrated that the difference in the data based on these two different drift-correction methods is generally minor. This demonstrates the validity of both approaches. As the equilibrium level at T_{ref} is more stable for loop-wise corrected data, this correction is applied to all linear data. Nonlinear data is corrected with the individual drift-correction as the high-temperature equilibrium values are more steady in this case.

The drift rate r_1 shows temperature-dependent behavior (see Fig. S11). For the storage contribution, the drift rate is rather constant for $T_f \leq T_{ref}+1.5\,\mathrm{K}$ and intensifies with increasing temperature.

a)

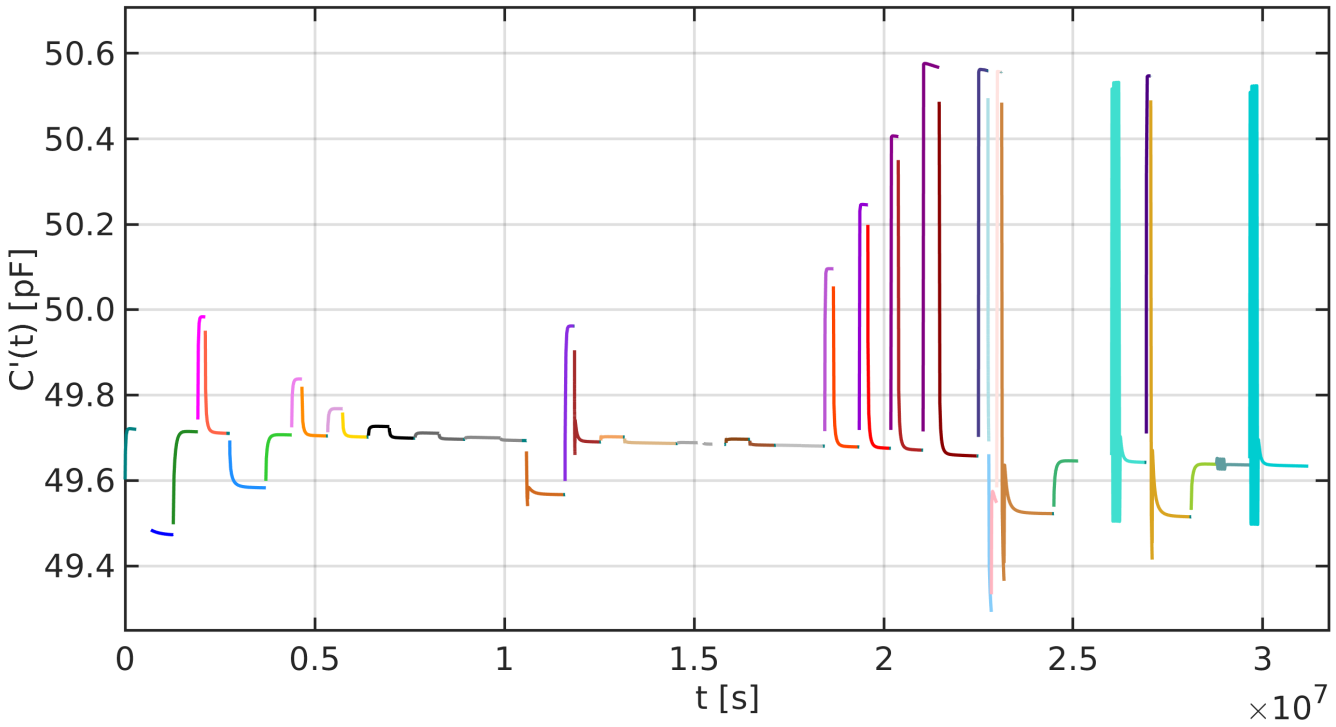

b)

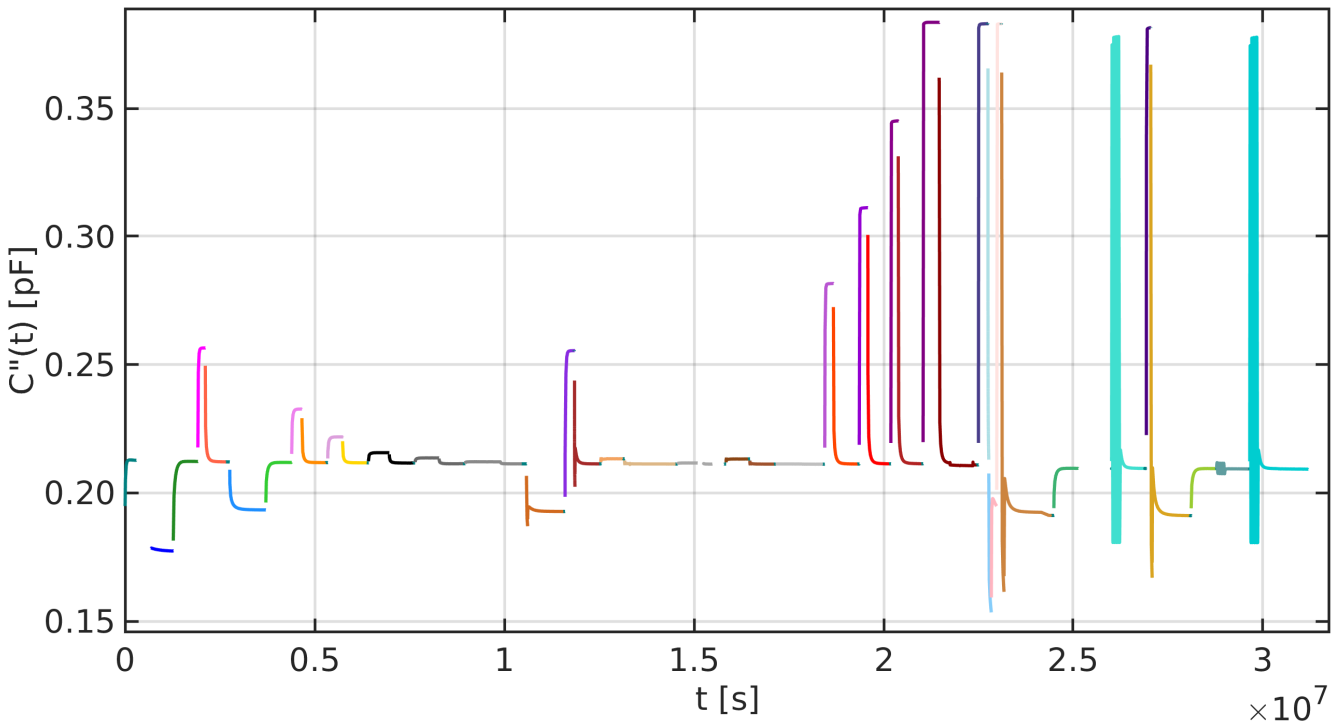

FIG. S9: Overview on the consecutive physical-aging experiments based on the temperature protocol presented in the main manuscript without drift correction for both storage (a) and loss (b) contribution of the measured capacitance.

a)

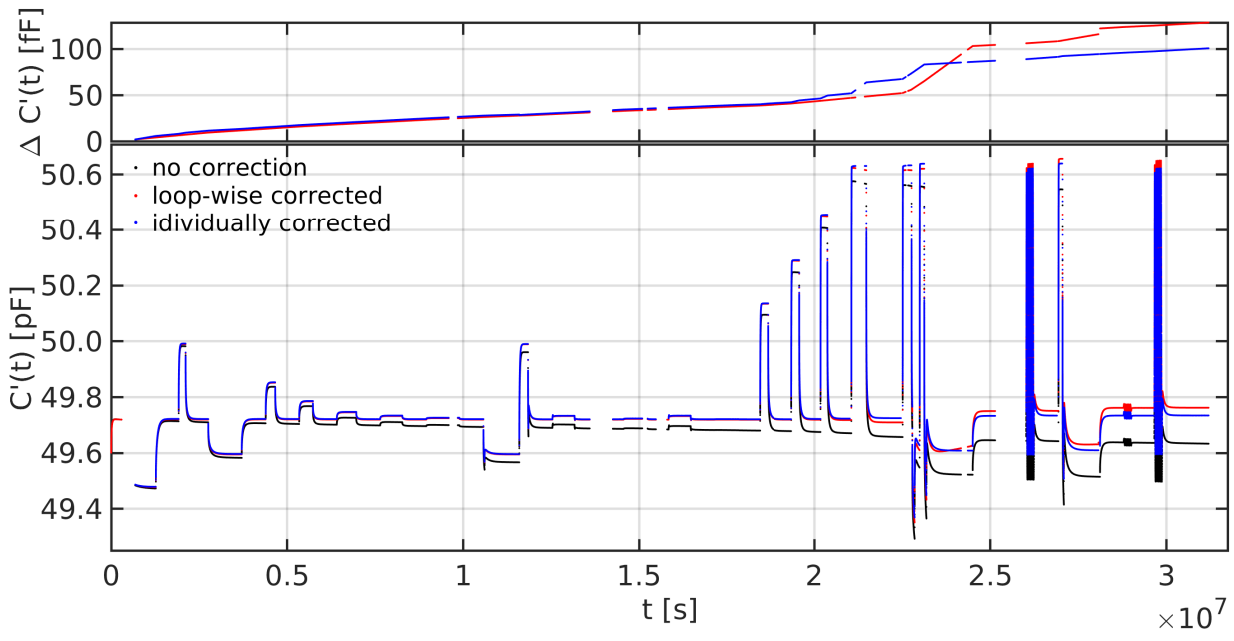

b)

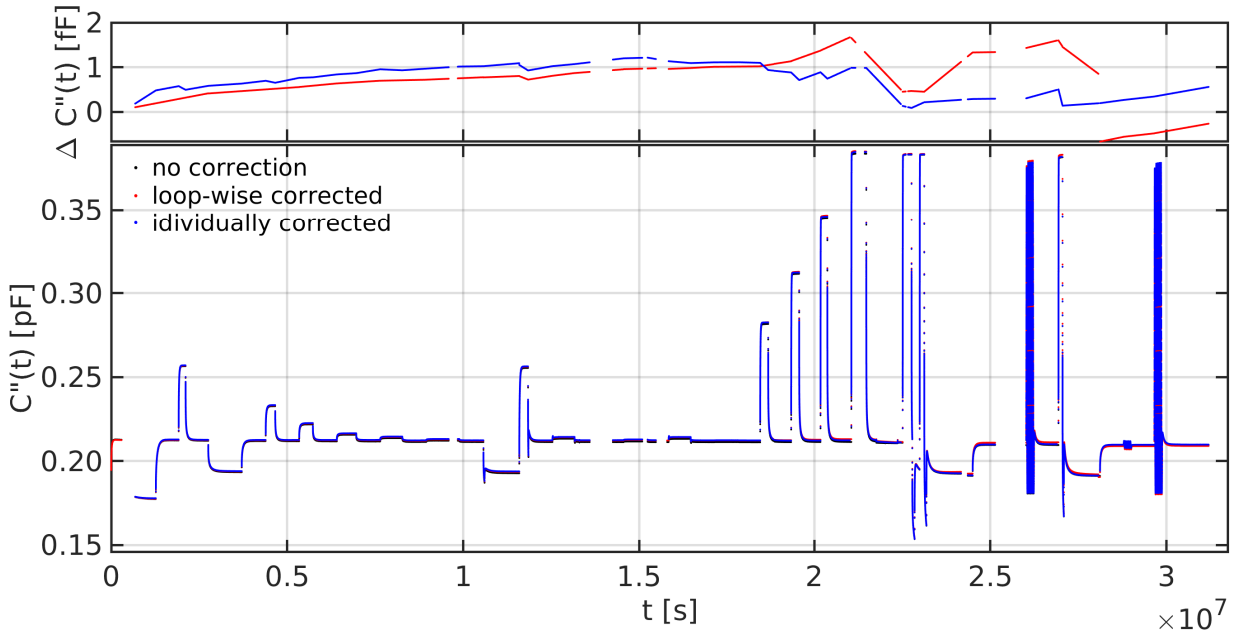

FIG. S10: Comparisons for uncorrected, individually drift-corrected, and loop-wise dirft-corrected data of the storage (a) and loss (b) contribution of the measured capacitance. Upper panels in a) and b) show the difference between un-corrected data and individually corrected (blue) or loop-wise corrected data (red).

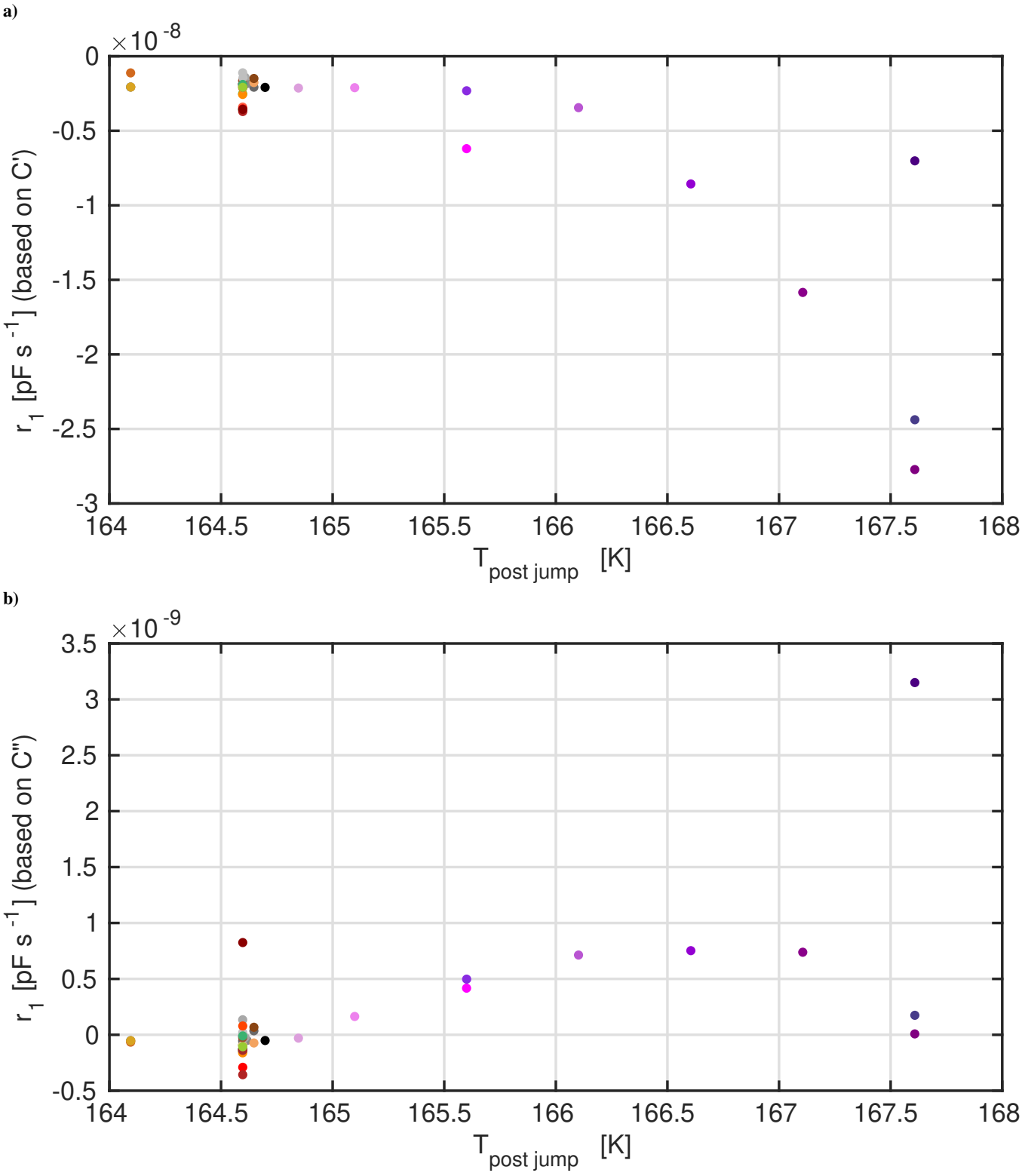

FIG. S11: Temperature-dependence of the drift rate r_1 for the storage (a) and loss (b) contribution of the measured capacitance based on the individual drift correction. The colors indicate the individual jumps, see Fig. S9.

b. equilibrium values of the measured quantity X_{eq}

A sample that is held at constant temperature can typically be regarded as being in equilibrium when the response levels off at a constant value in the long-time limit after a temperature jump. At that stage, the physical aging process is concluded and the material reflects te properties of the supercooled liquid. In the experiments, however, this long-time limit is rather characterized by a linear response behavior with a very small slope, i.e. the drift, as described in the previous section. The equilibrium values of the storage and loss response at a given temperature T_f are determined from the drift-corrected data as the mean value of the data interval that was used to determine the drift. The equilibrium data were interpolated by a non-linear polynomial function as indicated in Fig. S12. These data only weakly depend on the applied drift-correction method, as evident from the parameters in table S1. Thus, the individually drift-corrected data and fits are chosen to represent the temperature-dependence of X_{eq}. On the basis of low-temperature data a linear extrapolation was made that allows for an estimation of X_{eq} at $T \leq 163.5$ K.

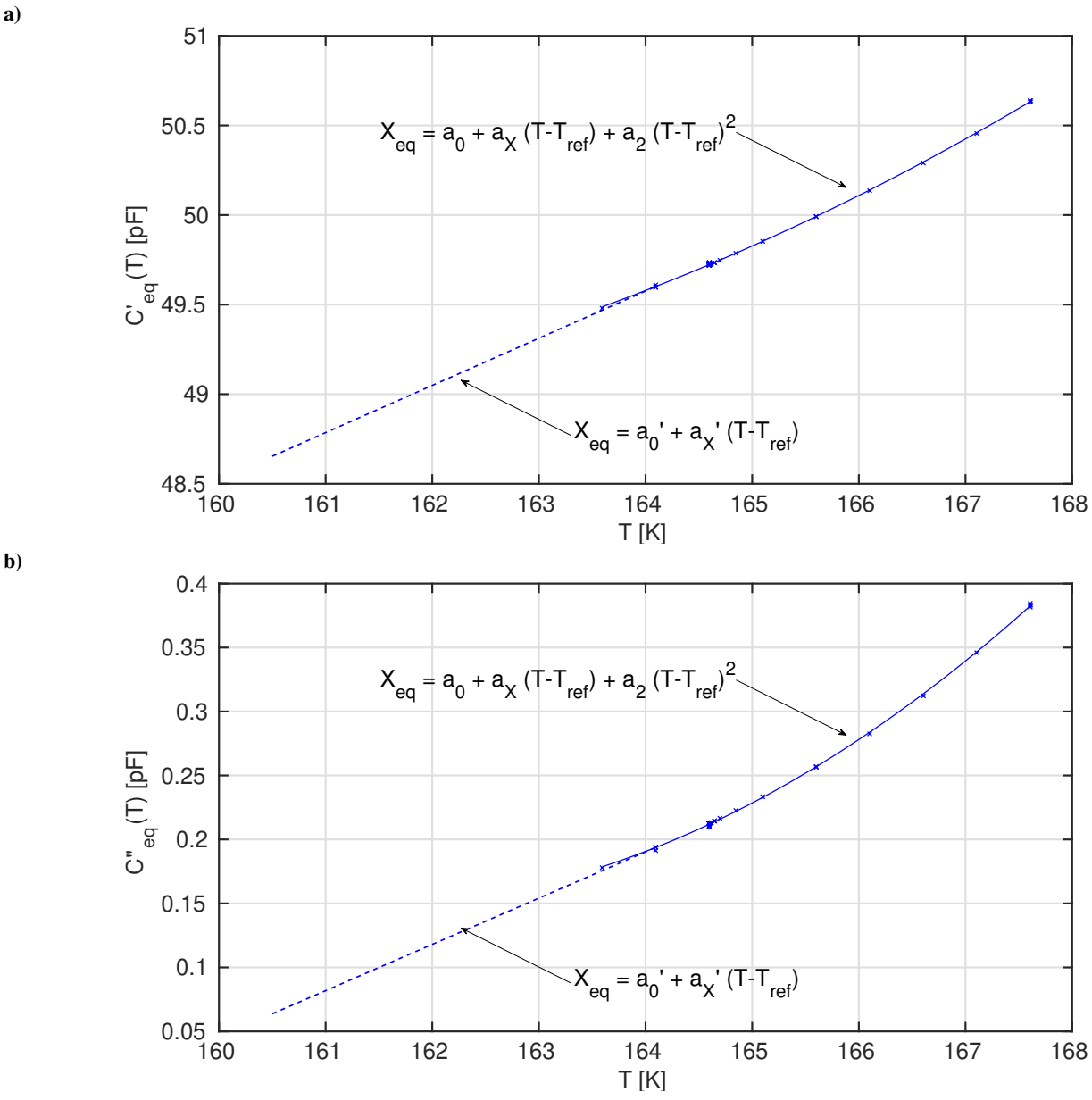

FIG. S12: Equilibrium responses X_{eq} in form of equilibrium values of storage (a) and loss (b) capacitance as functions of temperature for individually-corrected data. Full lines correspond to nonlinear interpolations of the data. Dashed lines represent linear extrapolations based on the existing data between 163.5 K and 164.5 K.

	$X = C'$ [pF]		$X = C$" [pF]	
	indvl. corr.	loop-wise corr.	indvl. corr.	loop-wise corr.
a_0 [pF]	49.7230	49.7251	0.2118	0.2117
a_X [pF K$^-$1]	0.2516	0.2493	0.0390	0.0390
a_2 [pF K$^-$2]	0.0168	0.0165	0.0059	0.0060
a'_0 [pF]	49.7332	49.7366	0.2119	0.2119
a'_X [pF K$^-$1]	0.2635	0.2640	0.0362	0.0363

TABLE S1: Parameters for nonlinear interpolation and linear extrapolation of individual and loop-wise corrected equilibrium data, X_{eq}, of storage and loss part of capacitance.

	$X = C'$ [pF]		$X = C$" [pF]	
	indvl. corr.	loop-wise corr.	indvl. corr.	loop-wise corr.
t_1 [-]	0.1697	0.1690	0.2102	0.2112
t_2 [K$^-$1]	0.0213	0.0212	0.0360	0.0362
t_3 [K$^-$1]	-0.0083	-0.0078	-0.0188	-0.0193

TABLE S2: Parameters for extrapolation along T_i and T_f of individual and loop-wise corrected data for the glassy response contribution, R_X^{eq}, of storage and loss part of capacitance.

c. glassy contribution of the measured quantity

When plotting the normalized response function, R_X^{gl}, the level of the data just after the initiation of the jump, i.e. at small $t - t_i$, is significantly lower than 1. Thus is due to the elastic contribution of the material and is possibly also influenced by secondary relaxation(s) that occur on time scales shorter than the time resolution of the experiment, i.e. at $t - t_i > 4$ s. This initital contribution is termed 'glassy contribution' in the following and it depends on both the initial temperature, T_i, and the final temperature,T_f, of a jump. The temperature dependence is fitted in the temperature ranges $T_{ref} - 1\,\mathrm{K} \leq T_i \leq T_{ref} + 1\,\mathrm{K}$ and $T_{ref} - 0.5\,\mathrm{K} \leq T_f \leq T_{ref} + 3\,\mathrm{K}$ by three free parameters t_1, t_2 and t_3 following $R_X^{gl} = t_1 + t_2 T_i + t_3 T_f$ (see table S2 for details on the parameters). Values connected to $T_i > T_{ref} + 1$ K are excluded from the fit as the initial plateau is not sufficiently captured for jumps from elevated temperatures, resulting in an excess value of R_X^{gl} as it includes a relaxational contribution. The deviations between fits of individually corrected and loop-wise corrected data are small, thus the individually corrected data represents the temperature dependence of R_X^{gl} in Fig. S13.

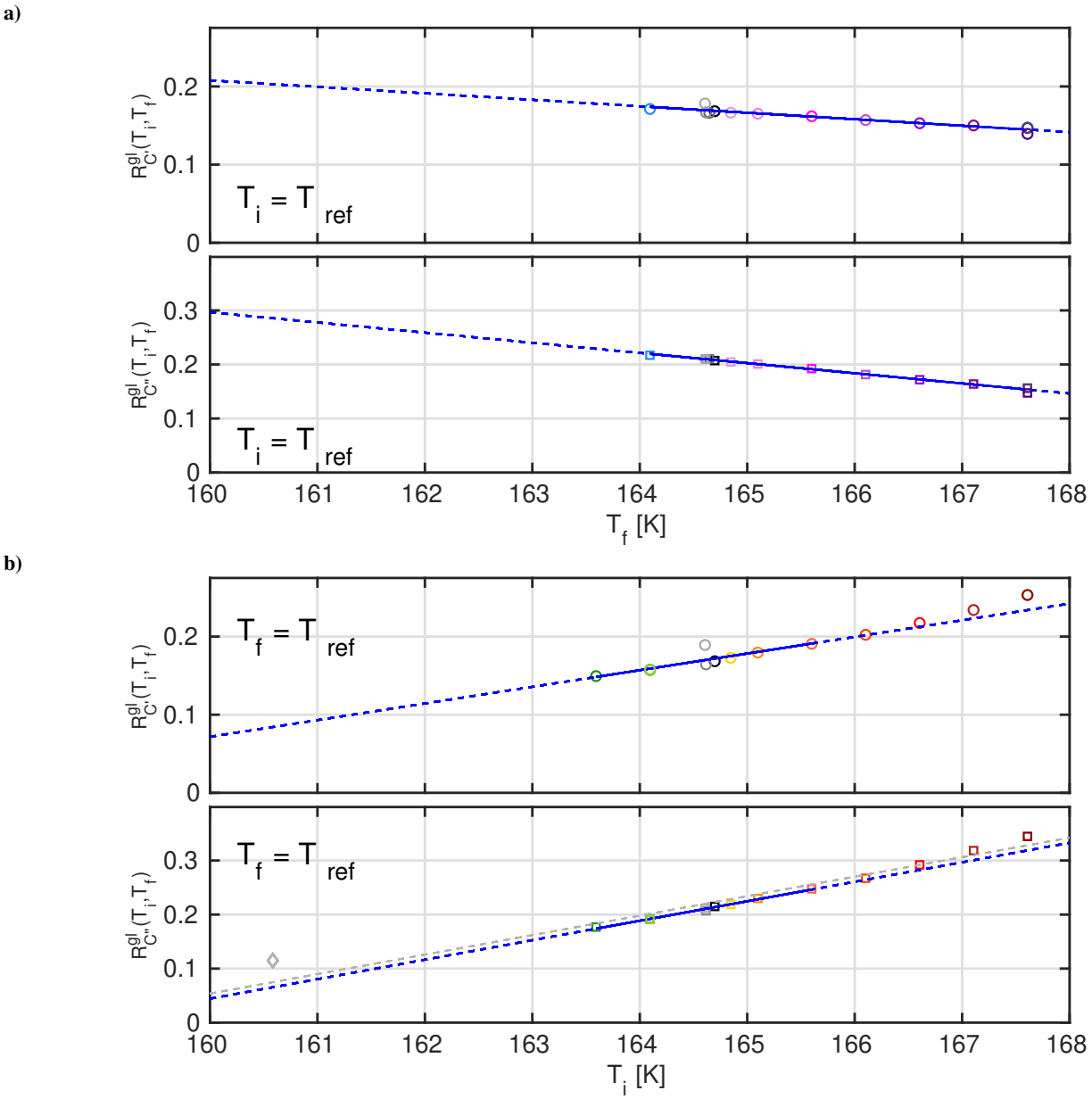

FIG. S13: Temperature-dependence of glassy response contribution, $R_X^{gl}(T_i, T_f)$. a) $R_X^{gl}(T_i = T_{ref}, T_f)$ for jumps starting starting at T_{ref}. b) $R_X^{gl}(T_i, T_f = T_{ref})$ for jumps ending at T_{ref}. Full lines represent the interval that is used for the fit, while dahes lines represent the extrapolation to the full temperature range. The grey dased line in the lower panel of b) represents the extrapolation of the glassy response contribution for jumps from temperatures T_i to T_f =164.1 K, i.e. $R_X^{gl}(T_i, T_f = T_{ref} -)0.5$ K. The grey diamond reflects the value of R_X^{gl} that is applied for the second jump of the 7 K double-jump protocol in Fig. S8d).

d. equilibrium values of the relaxation rate γ_{eq}

Fig. S14 shows extrapolations by Vogel-Fulcher-Tamman (VFT), a parabolic and the Aramov functions that are based on the loss-peak frequencies of the spectra shown in Fig. S1.

VFT function $\log_{10}\gamma_{eq}(T) = u_1 - u_2/(T-u_3)$ with u_1 =18.1, u_2 =791 K, and u_3 =130 K.

Parabolic function $\log_{10}\gamma_{eq}(T) = v_1 - v_2^2 * (1/T - 1/v_3)^2$ with v_1 =6.20, v_2 =2500 K^2, and v_3 =210 K.

Aramov function $\log_{10}\gamma_{eq}(T) = w_1 - \frac{(w_2/T)^{w_3}}{\ln(10)}$ with w_1 =10.4, w_2 =275 K, and w_3 =6.89.

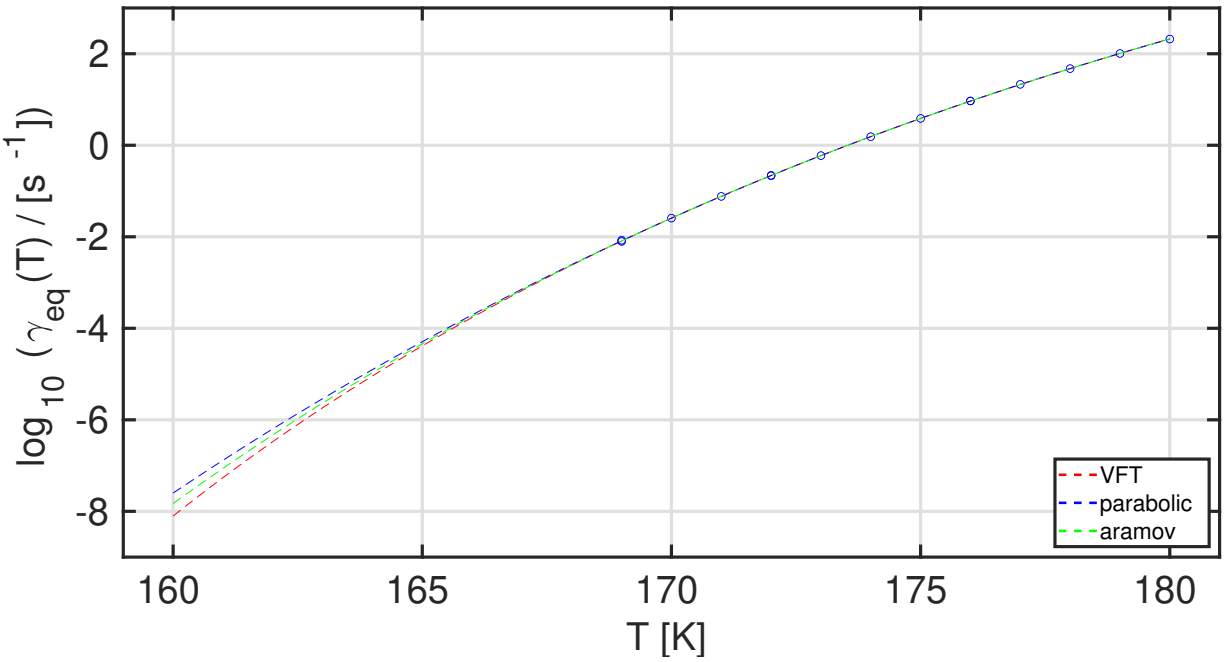

FIG. S14: Temperature-dependence of inverse time-scale derived from spectral loss-peak positions γ_{eq} and extrapolation based on Vogel-Fulcher-Tamman (VFT), parabolic and Aramov functions.

3. Evaluation of prediction-related quantities and details on double-jump temperature protocol

This section covers:

a) Connection of time increments for two individual jumps in the material-time formalism

b) Determination of Λ

c) Check on equilibrium clock rate γ_{eq}

a. Connection of time increments for two individual jumps in the material-time formalism

On the basis of the time-dependent aging rate,

$$\gamma(t) = d\xi(t)/dt, \tag{s4}$$

and the single-parameter aging ansatz according to which the aging rate is controlled by the measured quantity $X(t)$ itself,

$$log\gamma(t) - log\gamma_{eq}(T) = \Lambda \times (X(t) - X_{eq}(T)), \tag{s5}$$

we get the following equation for the time-dependent aging rate:

$$\gamma(t) = d\xi(t)/dt = \gamma_{eq}(T) \cdot \exp[\Lambda \times \Delta X(t)]. \tag{s6}$$

Thus,

$$d\xi(t) = \gamma_{eq}(T) \cdot \exp[\Lambda \times \Delta X(t)]\, dt \tag{s7}$$

and we can relate the incremental time step, dt, of two different individual jumps, A and B, by assuming that $d\xi(t_A^*) = d\xi(t_B^*)$ is valid at the specific points in time, t_A^* and t_B^*, and that $R_A(t_A^*) = R_B(t_B^*)$, so that:

$$dt_B^* = \frac{\gamma_{eq}(T_{f,\,A})}{\gamma_{eq}(T_{f,\,B})} \exp[-\Lambda \times (\Delta X_B - \Delta X_A) R_A(t_A^*)]\, dt_A^* \tag{s8}$$

b. Determination of Λ

For two jumps, A and B, going to the same final temperature and thus having the same equilibrium clock rates, i.e. $\gamma_{eq}(T_{f,\,A}) = \gamma_{eq}(T_{f,\,B})$, eq. s8 simplifies to:

$$dt_B^* = \exp[-\Lambda \times (\Delta X_B - \Delta X_A) R_A(t_A^*)]\, dt_A^* \tag{s9}$$

Thus, for a pair of two response data sets based on jumps ending at the same T_f, only the constant Λ is unknown and can be determined by minimizing the difference between the left-hand and right-hand sides of eq. s9 with Λ as a free fitting parameter. This procedure ist applied twice for each pair of jumps, i.e. for [A B] and [B A], that fulfills the stated requirement regarding T_f. The results for Λ based on individually corrected data are plotted in Fig. S15.The mean of the resulting values, Λ =91, is used for predicting the aging response. Only values above a threashold of 40 are taken into account: For pairs of jumps with very similar initial temperatures, $T_{i,A}$ and $T_{i,B}$, the fits seem less reliable and result in significantly lower values for Λ. These are excluded from the analysis.

c. Check on equilibrium clock rate

For two individual jumps, A and B, the relation between their incremental time steps, dt_A^* and dt_B^*, can be described by eq. s8. If one of these jumps ends at the reference temperature T_{ref}, the normalized equilibrium clock rate can be written as $\gamma_{eq,N}(T_{f,\,B}) = \frac{\gamma_{eq}(T_{f,\,B})}{\gamma_{eq}(T_{f,\,A}=T_{ref})}$. Using the extrapolation of gamma-values based on spectral data, we can check how well a fit of $\gamma_{eq,N}(T_{f,\,B})$ relates to it. In this case the normalized clock rate $\gamma_{eq,N}(T_B)$ is the only fitting parameter.

The normalized equilibrium clock rate that is connected to the fit of individual jumps is plotted in Fig. S16 together with the spectra-based clock rates that are normalized by the extrapolated value of γ_{eq} at T_{ref}.

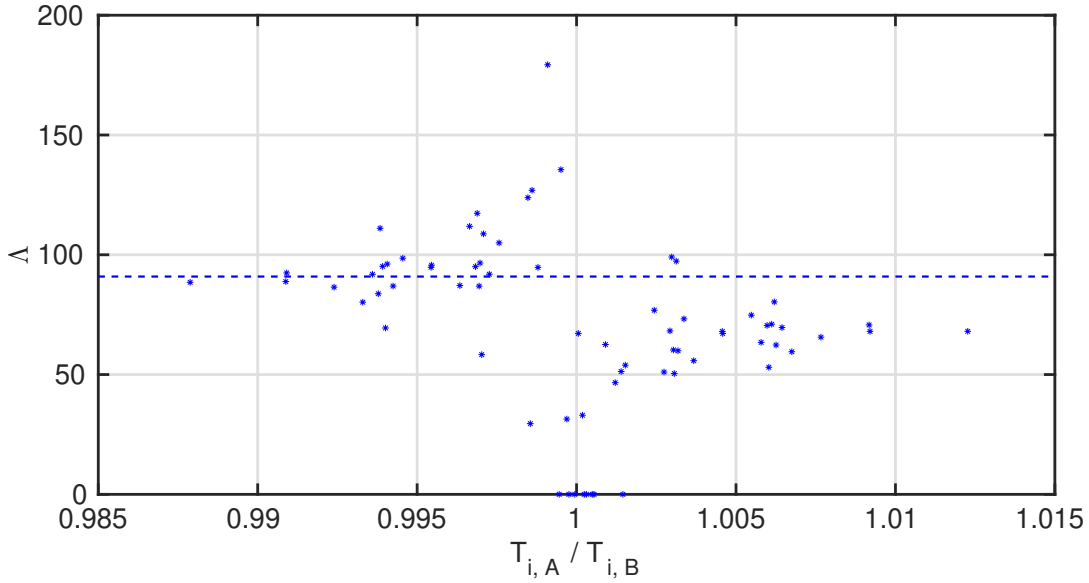

FIG. S15: Λ plotted as a function of temperature ratio $T_{i,A}/T_{i,B}$ for pairs of measured single temperature jumps sharing the same final temperature, T_f. The plot shows the analysis of Λ for individually corrected data.

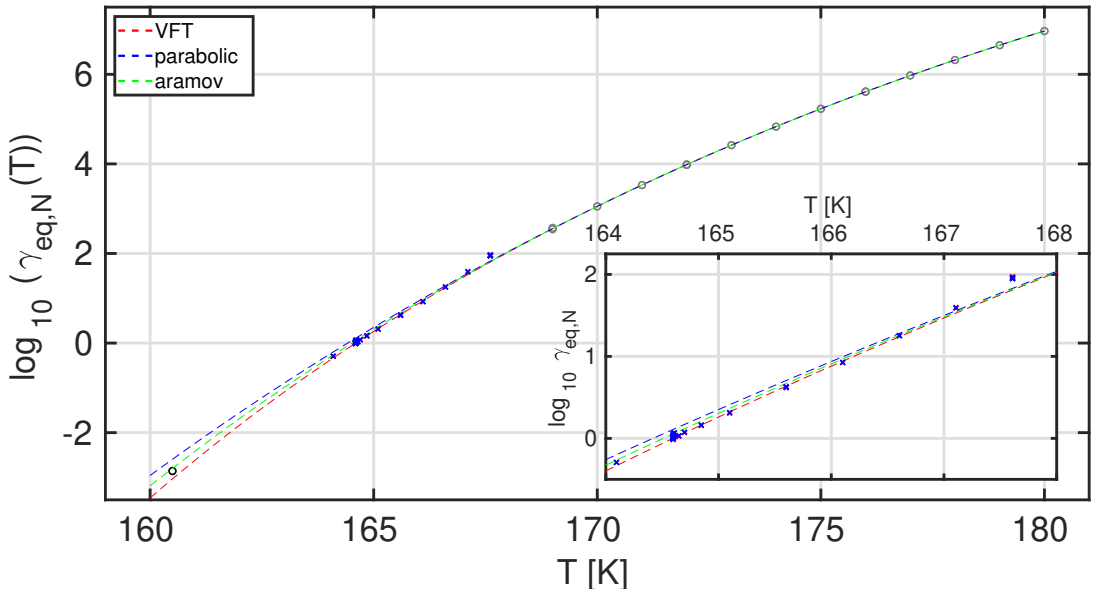

FIG. S16: Logarithmic normalized equilibrium clock rate, $\gamma_{eq,N}$ as a function of temperature. Dashed lines correspond to extrapolations (see legend for details) based on the clock rates determined from spectral data (grey cirles), crosses correspond to clock rates from fitting individual jumps for both loop-wise correction (red) and individual correction (blue). The inset shows a zoom of $\gamma_{eq,N}$ derived from individual jumps and extrapolations from spectral data.

4. Details on calculation of predictions

This section includes:

a) single temperature jumps

b) double temperature jumps

c) multiple temperature jumps

In order to calculate the prediction to a specific single temperature jump, the normalized response, $R_X(t)$, to another single temperature jump is used as a basis. This $R_X(t)$ is transformed in its response amplitude and in the duration of its time intervals to match the to-be-predicted data. This transformation occurs on the basis of the material-time aging formalism involving inter- and extrapolations of the equilibrium clock rate γ_{eq}, Λ, and the equilibrium response X_{eq}, as well as the inter- or extrapolation of the glassy contribution R_X^{gl}.
The basis data set for all the predictions shown in this work is a linear down-jump of 50 mK amplitude towards T_{ref}. However, we are not restricted to linear jumps as the formalism allows for making predictions on the basis of any jump, linear or nonlinear. For VEC, only predictions for storage data are presented.
In the following, the details of the calculation of the various predictions are given. To clarify which parameters or data are connected to the linear data set that serves as a basis for the predictions, these are marked by a triangle, e.g. $R_\triangle$ is the normalized response function for the linear jump of 50 mK amplitude that serves as a basis for the prediction, while R_X refers to the normalized response function for the to-be-predicted data set. As the basis data is a linear data set, its time can be referred to as material time ξ, where the individual data points of the data set are addressed by the index k. The time data connected to the to-be-predicted data can be refered to as laboratory time, t^{lab}. After the transformation of the material time to match the to-be-predicted data, the transformed time-data is refered to as the predicted time, t^{pred}.

a. Predictions: single temperature jumps

The following procedure describes the calculation of a prediction for an individual jump from T_i to T_f.
The response amplitude of the prediction, $\Delta X(\xi_k)$, is calculated from the normalized response function $R_\triangle(\xi_k)$ by:

$$\Delta X(\xi_k) = R_\triangle(\xi_k) \times \Delta X(0) \times \left(\frac{1 - R_X^{gl}(T_i, T_f)}{1 - R_\triangle^{gl}} \right), \tag{s10}$$

with the overall response amplitude $\Delta X = X_{eq}(T_i) - X_{eq}(T_f)$.

The time intervall of the prediction, dt_k, is calculated according to the material-time aging formalism by

$$dt_k = \frac{\gamma_{eq}(T_f)}{\gamma_{eq}^\triangle(T_f^\triangle)} \times \exp\left[-\Lambda \times \Delta X(\xi_k^\triangle, \xi_{k+1}^\triangle) \right] \times d\xi_k^\triangle, \tag{s11}$$

with $d\xi_k^\triangle = \xi_{k+1}^\triangle - \xi_k^\triangle$ and $\Delta X(\xi_k^\triangle, \xi_{k+1}^\triangle) = \frac{\Delta X(\xi_k^\triangle) + \Delta X(\xi_{k+1}^\triangle)}{2}$.
The predicted time is gained by

$$t_k^{pred} = \sum_{k=1}^{N} dt_k \tag{s12}$$

b. Predictions: double temperature jumps

The prediction of the response to a double jump experiment can be understood as the prediction of an individual jump for the initial jump of the double-jump protocol, and a superpositionof two individual jumps made in material time for the second jump of the protocol. For a visualization of this procedure, see Fig. S21.
The calculation of each of the double-jump predictions can be broken down into the two steps described above, i.e. the calculation of the response amplitude and the calculation of the time steps.
Starting with the initial jump, the response amplitude of the prediction can be calculated as in eq. s10. Then, the time steps are transformed from material time to the time as observed in the experiment as described in s11. However, this is not persued for

the complete jump, but is interrupted at the point where the second jump is initiated. This is the case, when the predicted time, t^{pred}, is equal to the last point in laboratory time of the initial jump, t^{lab}, of the to-be-predicted data set, just before the second jump is initialized.

Now the prediction for the second jump can be calculated. As the point in time of the jump is known for t^{obs}, it is also known at which material time ξ the jump occurs, which is denoted as ξ_2. As the prediction of the second jump is calculated from the superposition of the predictions for the individual jumps in material time, the response of that total prediction is given by

$$\Delta X_{tot}(\xi_k^{\triangle}) = \Delta X_1(\xi_k^{\triangle} - \xi_2^{\triangle}) + \Delta X_2(\xi_k^{\triangle}). \tag{s13}$$

The transformation from material time to t^{pred} is analogous to the approach described for individual jumps in eq. s11, where ΔX has to be replaced by ΔX_{tot} from eq. s13.

c. Predictions: multiple temperature jumps

The prediction of a response that involves multiple jumps is very similar to the prediction of a double jump: the approach iteratively determines the response amplitude of a prediction by superposition of the individual responses in material time up to the point of the next temperature jump, which is defined by the temperature protocol itself, followed by the transformation of the time step from material time to t^{pred} in order to match the laboratory time of the to-be-prdicted experiment. The significant difference is, that the superposition in material time involves more than two individual predictions.

Supplementary Information B: Overview on the data set measured on NMEC

This section contains

a) spectra of the storage and loss dielectric permittivity

b) temperature-dependent data-set of the storage and loss capacitance at $\nu = 10$ Hz

c) comparisons of the experimental response (storage part of capacitance) with predictions for single and double-jump temperature protocols in the linear ($\Delta T \leq 100$ mK) and nonlinear ($\Delta T > 100$ mK) regime

a. Spectra of storage and loss dielectric permittivity for NMEC

All data shown for NMEC were measured on a single sample measured by a capacitor with a geometric capacitance $C_{geo} = 15.7$ pF. This sample was initially quenched to $T_{cryo} = 167$ K by insertion into the pre-cooled cryostat and was held at that temperature to equilibrate. Subsequently, the spectra presented in Fig. S17 were measured while tracking the temperature-specific voltage of the micro-regulator, which was then used to calibrate the temperature-control of the micro-regulator.

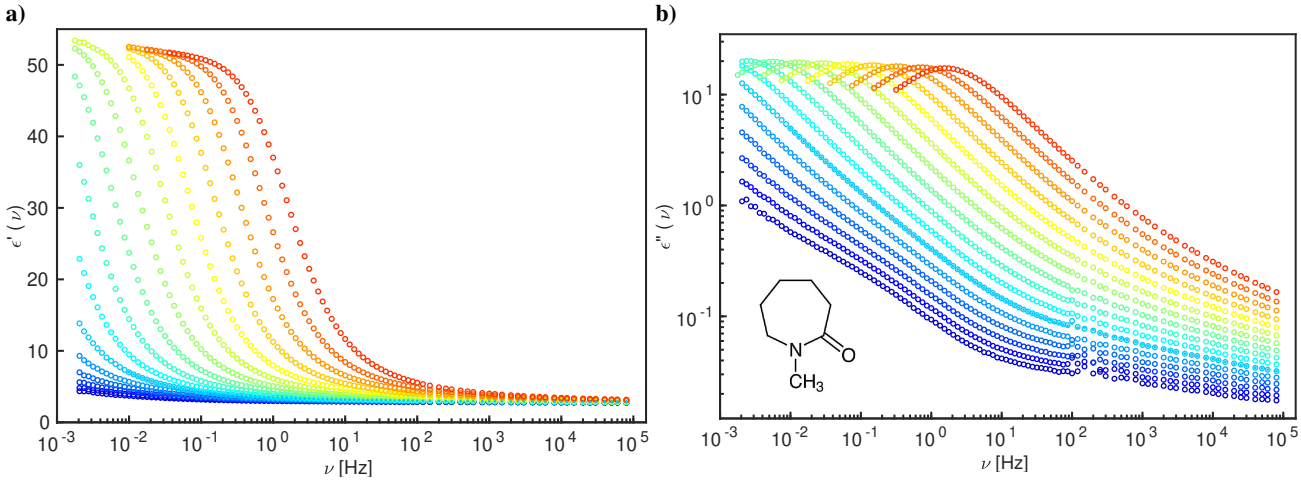

FIG. S17: Dielectric spectra for NMEC. (a) Storage and (b) loss capacitance as functions of frequency, $\varepsilon'(\nu)$ and $\varepsilon"(\nu)$, measured by means of a high-precision custom-built frequency generator and a commercial LCR meter in a temperature range from 165 K to 180 K in 1 K steps. The inset in panel (b) depicts the skeletal formula of NMEC.

b. Overview on storage and loss capacitance data for NMEC

After the measurements of the spectra, the micro-regulator was activated and set to $T = T_{MR} = 166$ K. By means of a Andeen-Hagerling ultra-precision capacitance bridge (model 2700A) the capacitance, C, and the dielectric loss, $\tan\delta$, were tracked at a frequency of $\nu = 10$ Hz. Individual temperature jumps with amplitudes from $\Delta T = 5$ mK up to 3 K were initiated, as well as double-jump protocols with ΔT_1 =-50 mK and $\Delta T_2 = -\Delta T_1/2$. An overview of the temperature protocol is shown in Fig. S18 together with the corresponding storage and loss capacitance. However, the first four jumps were measured with the conventional dielectric setup that was also used for the measurements of the spectra in Fig. S17. These data visualize the significantly higher accuracy of measurements with the Andeen-Hagerling AH2700. After ca. 35 weeks of consecutive measurements, a failure in the cooling-unit of the cryostat terminated the measurement sequence.
The reponse of individual temperature jumps is plotted against logarithmic time in Fig. S19. The initital 10 s of each jump are clearly still influenced by the temperature regulation and are excluded from the analysis. After this thermalization, the initial plateau is only captured for jumps from $T < T_{ref}$ to higher temperatures (purple colors in Fig. S19a)), while for all other jumps a significant amount of relaxation has taken place, so that the data set on NMEC does not allow for an analysis of the glassy contribution. Note the difference in signal-to-noise ratio for the conventional dielectric setup and the Andeen Hagerling that becomes obvious in the fourth jump of the data set (T_{ref} to $T_{ref}+3$ K, red color), where the measurement setups were switched. Fig. S19b) depicts individual temperature jumps with temperature amplitudes between 5 mK and 100 mK that correspond to the data magnified in the insets of Fig. S18.

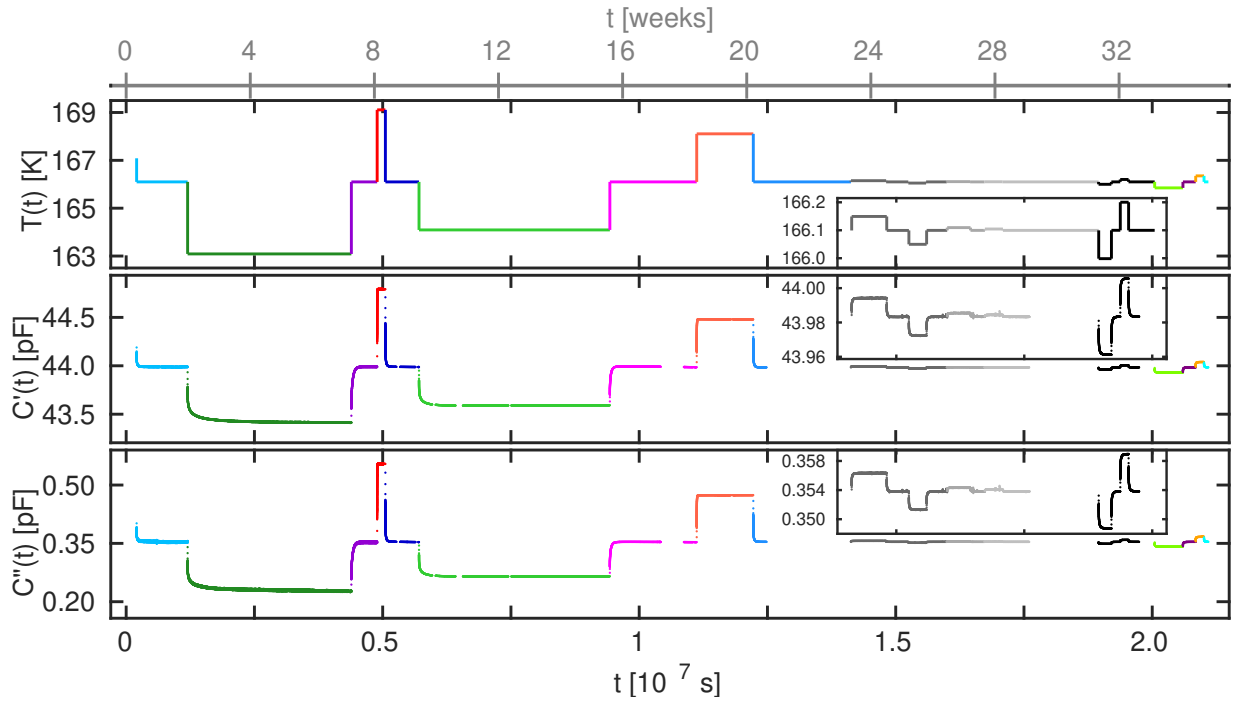

FIG. S18: Overview of the temperature protocol and raw data of the full experiment on NMEC after a loop-wise drift correction. The temperature protocol of experiments realized by modulations around $T_{ref} = 166.1$ K is plotted in the upper panel together with the real and loss part of the measured capacitance $C(\nu = 10\,\mathrm{Hz})$ in the lower panels, each as functions of time on a linear scale in seconds and in weeks. Jumps larger than 100 mK are colored while jumps of 100 mK or less are depicted on a grey scale. The insets show details of jumps with $\Delta T \leq 100$ mK and share the same time-axis as the main panels.

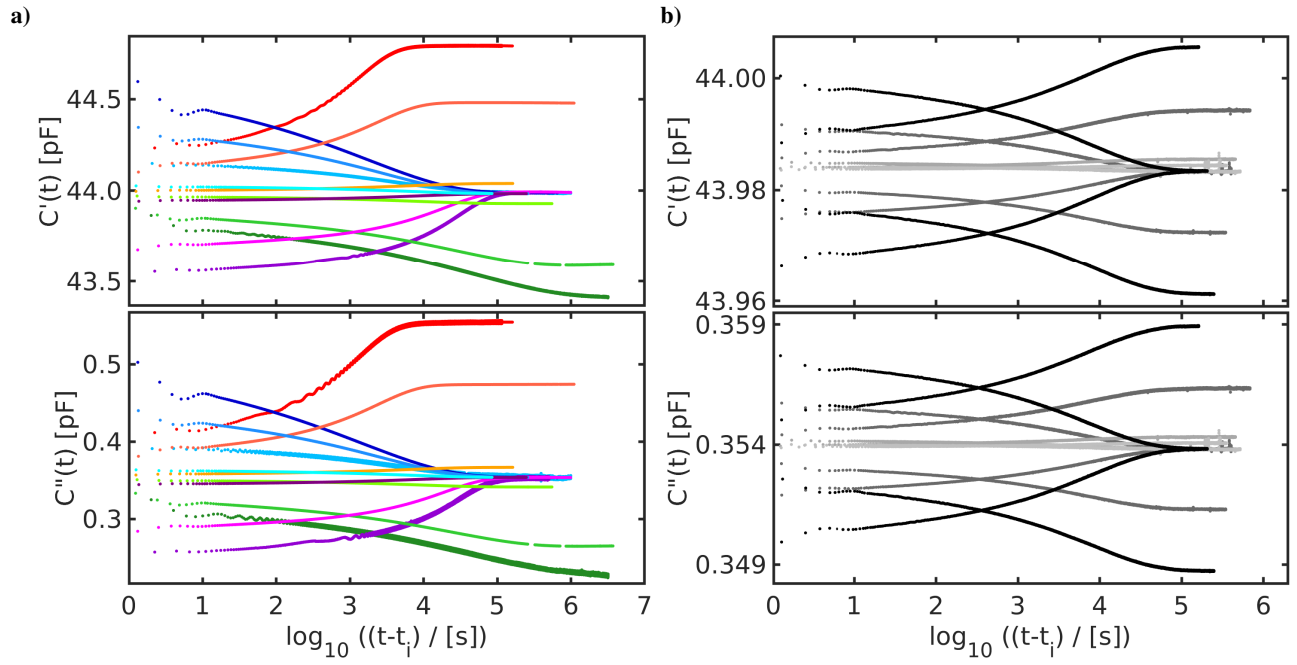

FIG. S19: The storage and loss capacitance data, $C'(\nu = 10\,\mathrm{kHz})$ and $C''(\nu = 10\,\mathrm{kHz})$, are plotted as functions of the logarithm of the time that has passed after the initiation of each jump. **a)** depicts jumps with $\Delta T > 100$ mK and **b)** is a zoom on jumps of 100 mK less.

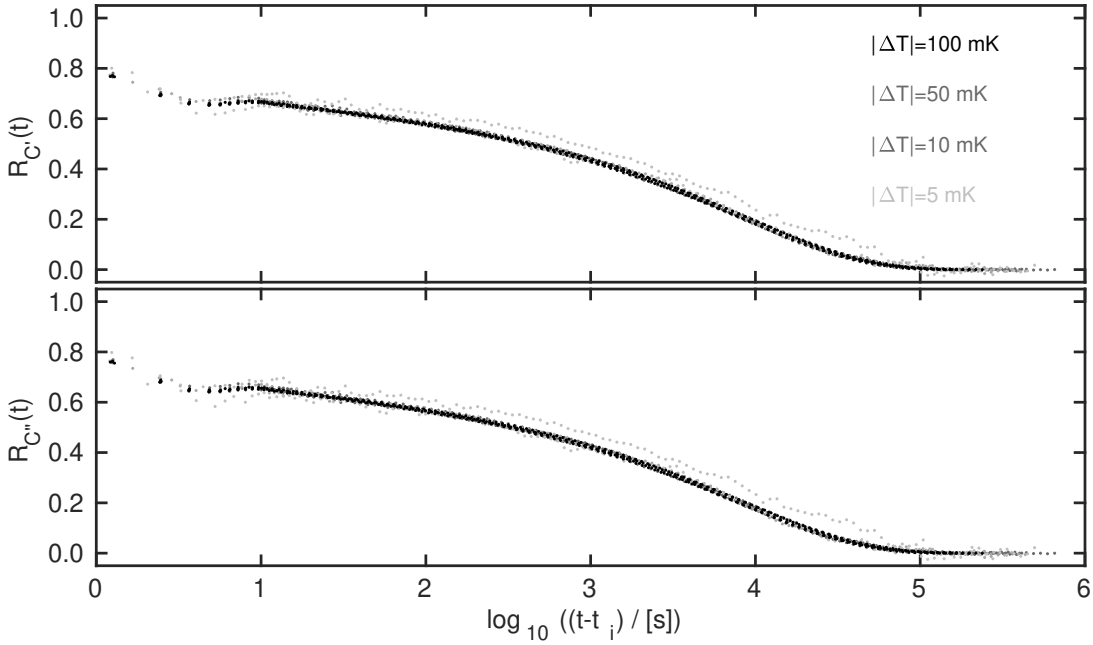

FIG. S20: Normalized relaxation function for real and loss part of capacitance data, $R_{C'}$ and $R_{C''}$, of single temperature jumps with amplitudes between 5 mK and 100 mK.

In Fig. S20, these linear aging data are plotted in a normalized representation. Data with amplitudes down to 10 mK collapse as expected for linear relaxation. The response to 5 mK-jumps show deviations, assumably inidicating the low-amplitude limit of the applied temperature protocol.

c. *Comparison of experimental data and predictions for NMEC*

Fig. S21 visualizes the superposition of individual predictions to yield the prediction for a double-jump temperature protocol on the example of experimental data. This example covers a double-jump temperature protocol in the linear regime with ΔT_1 =-50 mK and ΔT_2 =+25 mK. In a), the storage and loss capacitance are plotted against linear time. The same data are presented in the lower panel of c) (storage contribution only) and in d). See figure caption for details.

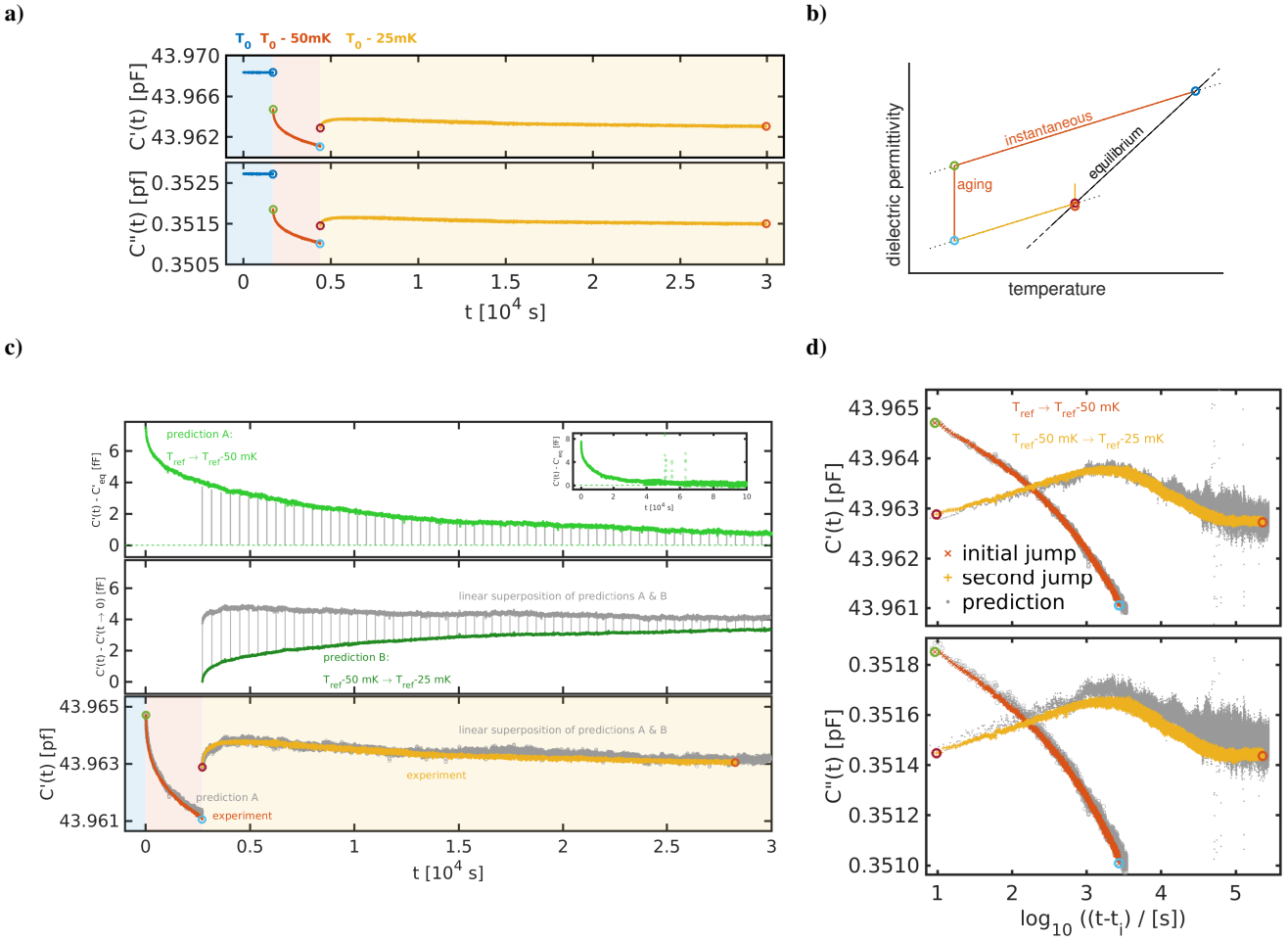

FIG. S21: Experimental data and prediction of a linear double jump on NMEC with ΔT_1 =-50 mK and ΔT_2 =+25 mK. a) As a function of linear time. (b) Schematic representation of a crossover experiment visualizing the glassy and aging contributions of the capacitance for two subsequent temperature jumps. Note that colored circles mark identical experimental situations for the different representations of the data throughout a) to d). c) Prediction of the experimental response based on an individual, independently measured linear temperature jump on the NMEC sample. top panel: Prediction of the dielectric aging response to a temperature jump from T_{ref} to $T_{ref}-50$ mK as a function of logarithmic time based on an individual jump from $T_{ref}+10$ mK to T_{ref} after subtraction of the equilibrium value, X_{eq}. Inset top panel: Prediction of aging response to temperature perturbation as a function of time as in main panel depicting the complete response towards equilibrium. Mid panel: Prediction of the dielectric aging response to a temperature jump from $T_{ref}-50$ mK to $T_{ref}-25$ mK as a function of time based on the same data as used for the prediction in top panel, after subtraction of the glassy contribution to the jump. Grey vertical lines reflect the same $\Delta C'(t)$ values at a given point in time from top panel to visualize the linear superposition of the two predicted curves that yield the prediction of the dielectric response of the second jump (dark grey data points). Bottom panel: Experimental response (storage data) plotted together with the prediciton from mid panel. d) The collapse of prediction and experimental data for both storage and loss contribution illustrate the applicability of linear superposition in the linear response limit.

The predictions and experimental responses to individual temperature jumps with amplitudes larger than 100 mK, i.e. nonlinear individual jumps, are plotted in Fig. S22. Note that the details of the aging responses are captured very accurately for down-jumps, while the predictions show more and more pronounced signs of deviation from experimental data for up-jumps with increasing amplitude, similar to the behiavior observed for VEC.

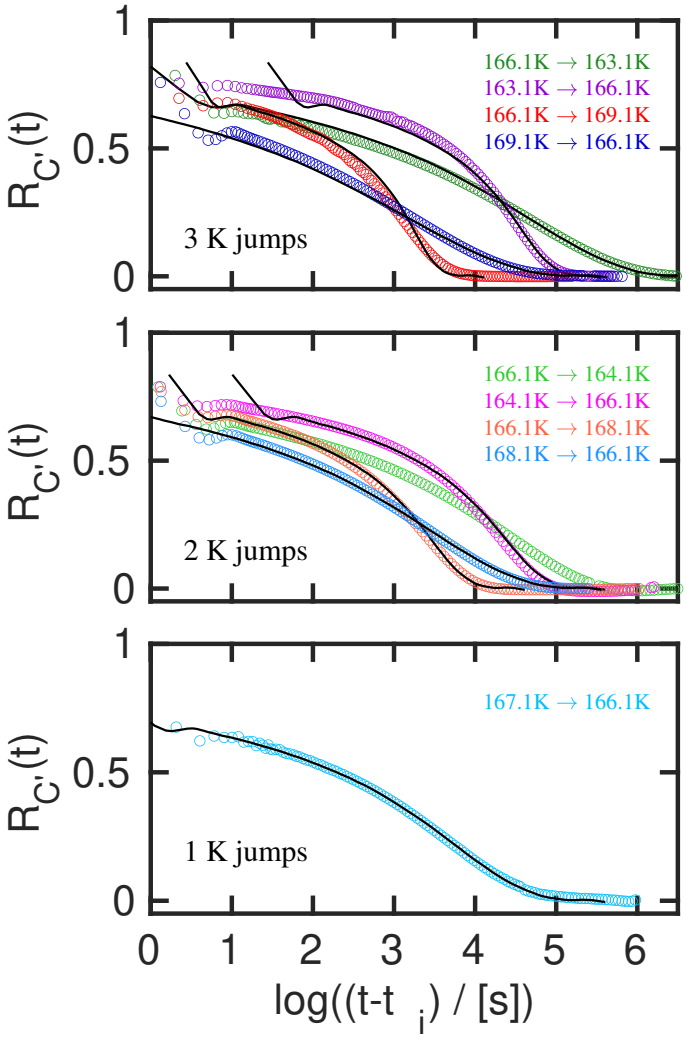

FIG. S22: Experimental data and predictions of nonlinear individual jumps on NMEC involving temperature jumps between 1 K and 3 K.

Supplementary Information C: Computer simulations

The simulations employed the Kob-Andersen 80/20 binary Lennard-Jones (LJ) mixture [40], which was simulated by means of standard NVT Nose-Hoover dynamics [46] using the GPU-optimized software RUMD [47]. A system of 8000 particles was simulated. In LJ units the time step was 0.0025. All pair potentials were cut and shifted at 2.5 times the length parameter σ_{ij} of the relevant LJ pair potential ($i, j = A, B$).

At the reference temperature $T = 0.60$ the potential-energy time-autocorrelation function was calculated as follows. First 10^7 time steps of simulations were carried out for equilibration. After that 100 configurations were picked out equally spaced in time from a production run of another 10^7 time steps, each of which were used as initial configurations for calculating the time-autocorrelation function.

The temperature jump simulations were carried out by the following procedure applied for all starting temperatures. First, 10^9 time steps were spent on equilibration at the given starting temperature. After that a total of 5×10^8 time steps were spent on the production runs. Equally spaced among these, 1000 configurations were picked out to serve as starting configurations for a temperature jump to $T = 0.60$. The data presented in Fig. 4 of the main paper represent averages of these 1000 jumps.